Supplementary Materials

A decade (2008-2017) of water stable-isotope composition of precipitation at Concordia Station, East Antarctica

Giuliano Dreossi[1,2], Mauro Masiol[1], Barbara Stenni[1], Daniele Zannoni[1], Claudio Scarchilli[3], Virginia Ciardini[3], Mathieu Casado[4], Amaëlle Landais[4], Martin Werner[5], Alexandre Cauquoin[6], Giampietro Casasanta[7], Massimo Del Guasta[8], Vittoria Posocco[1], and Carlo Barbante[2]

1. Department of Environmental Sciences, Informatics and Statistics, Ca' Foscari University of Venice, Mestre Venice, Italy
2. Institute of Polar Sciences, National Research Council of Italy (ISP-CNR), Mestre Venice, Italy
3. ENEA, Laboratory for Observations and Measures for the Environment and Climate, Rome, 00123, Italy
4. Laboratoire des Sciences du Climat et de l'Environnement, LSCE/IPSL, CEA-CNRS-UVSQ, Université Paris-Saclay, Gif sur Yvette, France
5. Alfred Wegener Institute (AWI), Helmholtz Centre for Polar and Marine Research, Bremerhaven, Germany
6. Institute of Industrial Science, The University of Tokyo, Kashiwa, Japan
7. Institute of Atmospheric Sciences and Climate, National Research Council of Italy (INO-CNR), Bologna, Italy
8. National Institute of Optics, National Research Council of Italy (INO-CNR), Sesto Fiorentino (FI), Italy

Correspondence to: Mauro Masiol (mauro.masiol@unive.it) and Barbara Stenni (barbara.stenni@unive.it)
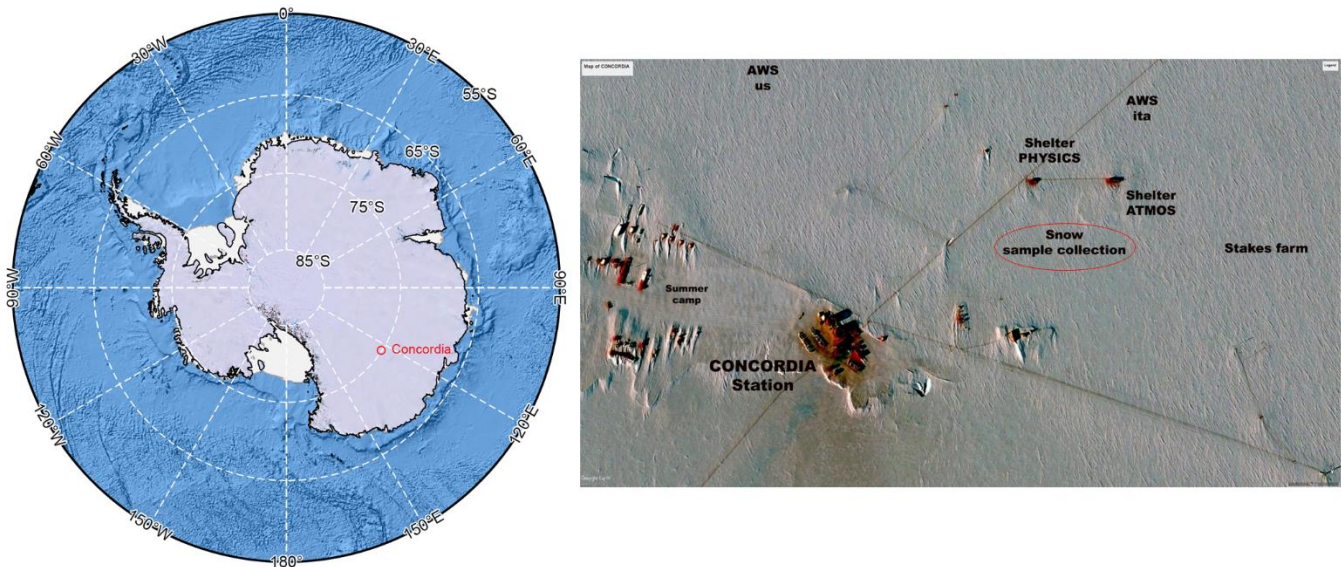
Figure S1. Map of Antarctica with the sampling location (left) and the snow sample collection position with respect to Concordia Station (right). The map (left) was drafted using (i) the ETOPO1, IBCSO, and RAMP2 data for basemap usage in Quantarctica3 (Matsuoka et al., 2021), (ii) the medium resolution vector polygons of the Antarctic coastline (2014) by the UK Polar Data Centre (Gerrish et al., 2020), and (iii) the Antarctic Ice Shelf Data by the U.S. National Ice Center (USNIC, https://usicecenter.gov/Resources/AntarcticShelf). The image on the right was modified from Google Earth (© Google Maps).
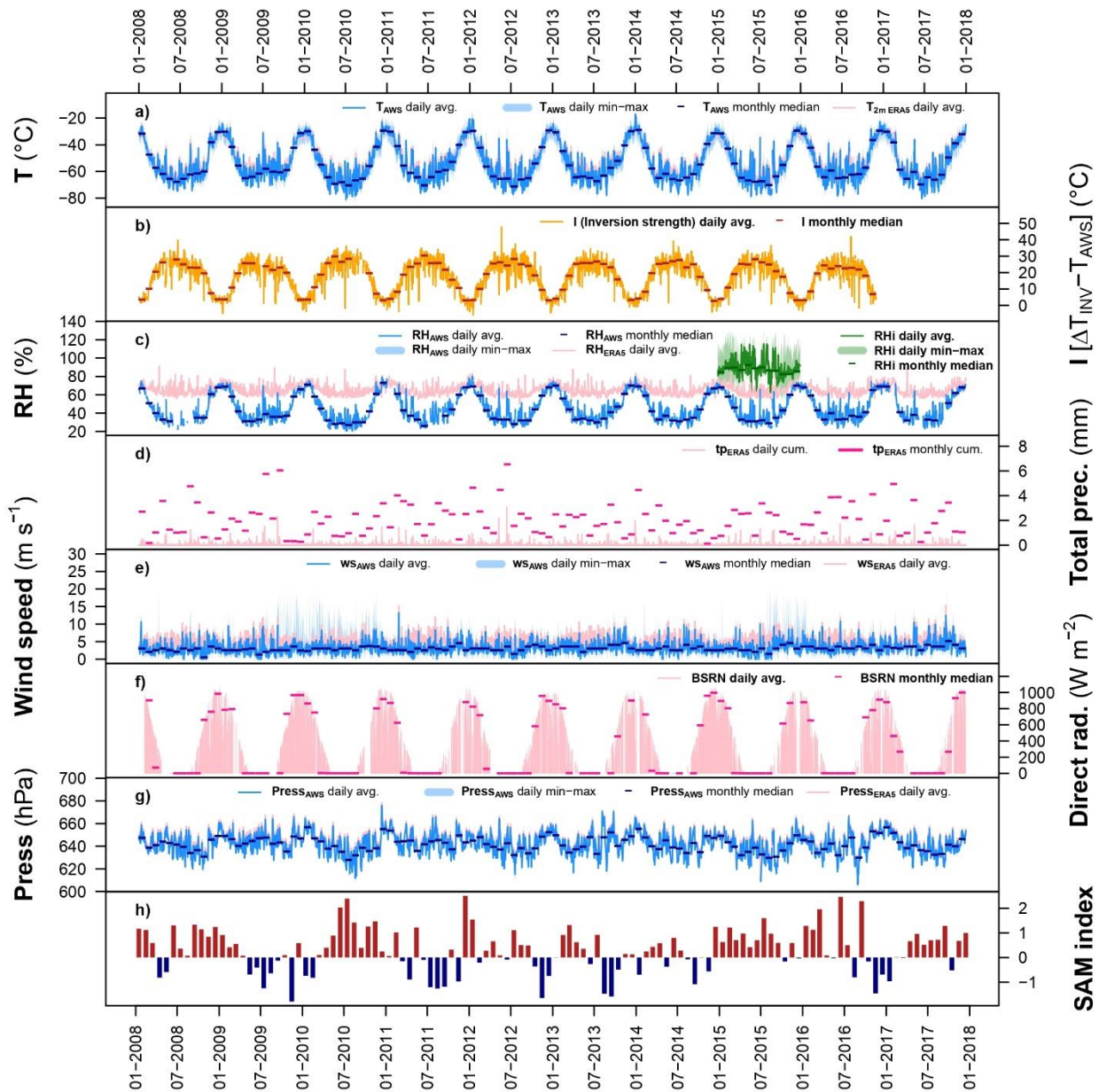
Figure S2. Daily and monthly averaged meteorological variables recorded during 2008-2017. Panel a) daily average and daily min-max AWS T_{2m} temperature (dark and light blue, respectively), monthly median (very dark blue) and daily average (pink) from ERA5. Panel b) daily average and monthly median inversion strength (yellow and red, respectively) calculated as the difference between AWS T_{2m} and inversion temperature from radiosounding data. Panel c) daily average and daily min-max AWS relative humidity (dark and light blue, respectively), monthly median (very dark blue) and ERA5 relative humidity daily average (pink). Panel d) daily and monthly cumulative total precipitation from ERA5 (light and dark pink, respectively). Panel e) daily average and daily min-max AWS wind speed (dark and light blue, respectively), monthly median (very dark blue) and ERA5 daily average wind speed (pink) Panel f) daily average and monthly median BSRN direct radiation (light and dark pink, respectively). Panel g) daily average and monthly median atmospheric pressure (dark and light blue, respectively), monthly median (very dark blue) and ERA5 daily average atmospheric pressure from ERA5 (light and dark pink, respectively). Panel h) monthly Antarctic Oscillation index (AAO, also known as Southern Annular Mode, SAM), with negative values in blue and positive ones in red. Daily averages are reported in local time.
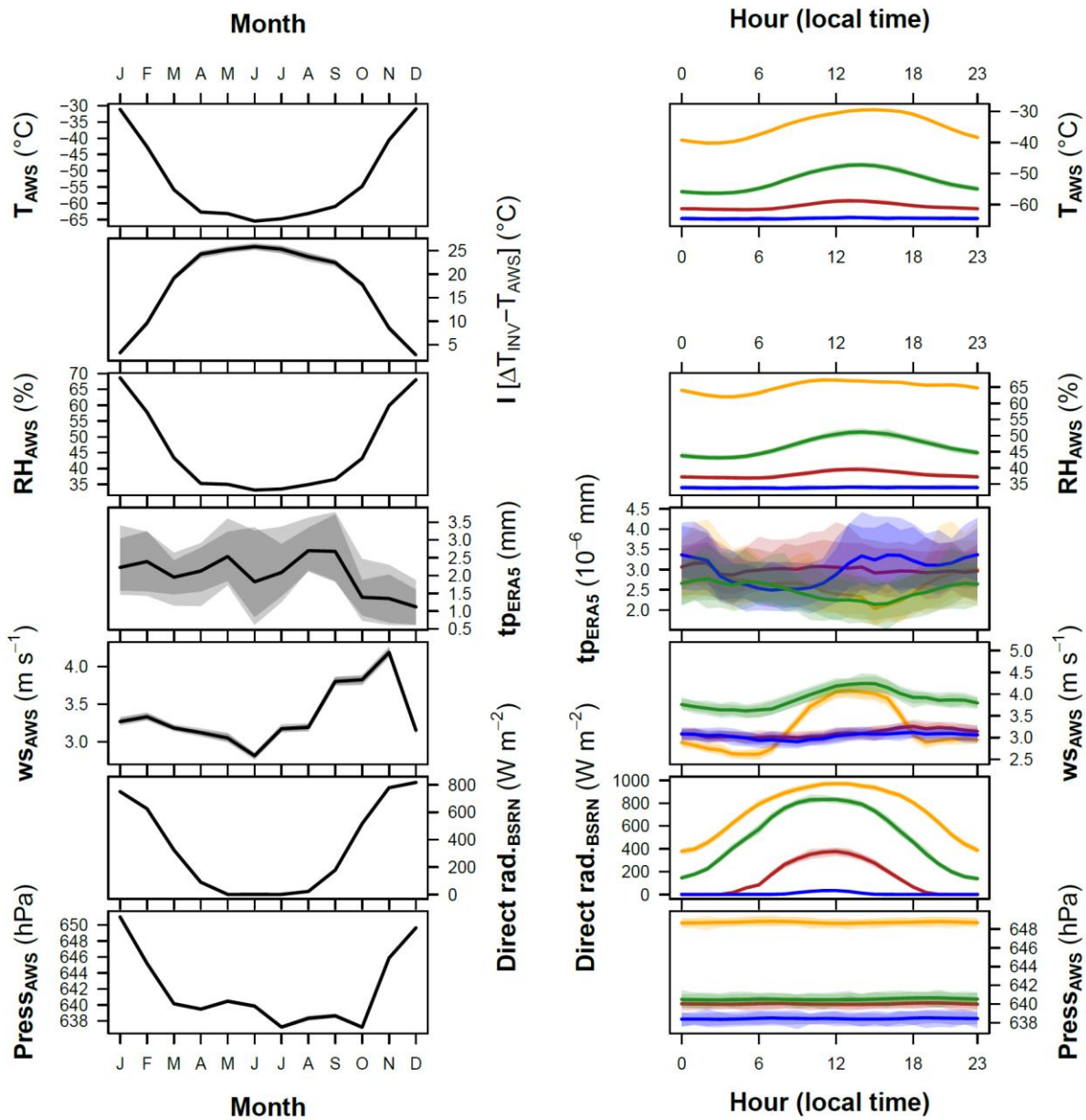
Figure S3. Monthly averaged (left) and hourly meteorological variables (right) recorded during 2008-2017 as measured by AWS or modeled by ERA5. Hourly patterns are calculated over different seasons: Austral winter (blue), spring (green), summer (gold) and autumn (brown); data reported in local time.
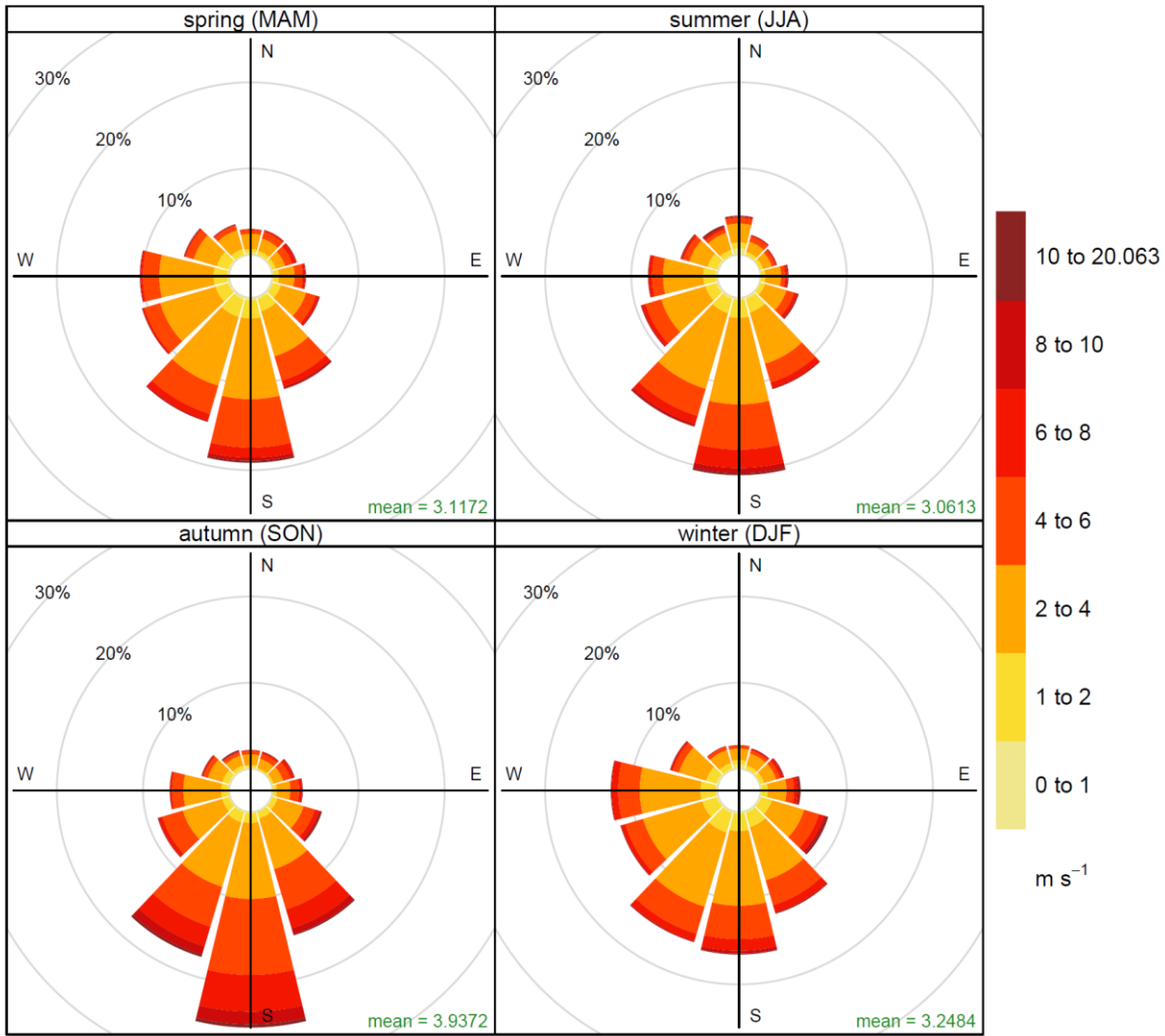
Figure S4. Seasonal wind roses calculated over the 2008-2017 period.
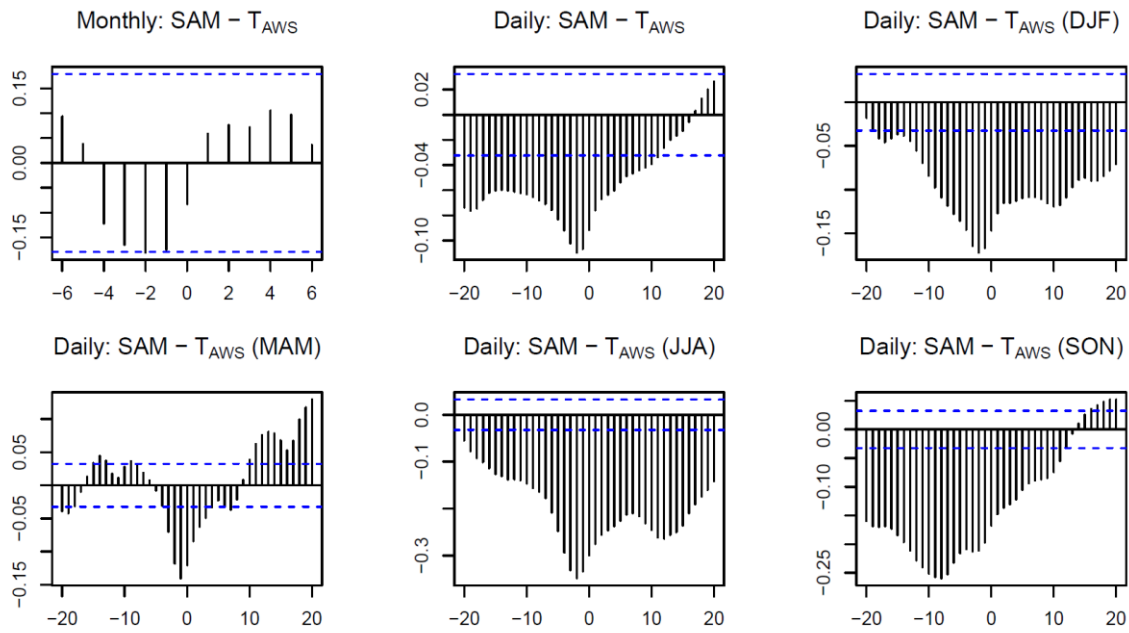
Figure S5. Cross-correlation functions on SAM index and air temperature measured by the AWS for monthly data, for total daily data and for daily data divided by each season.
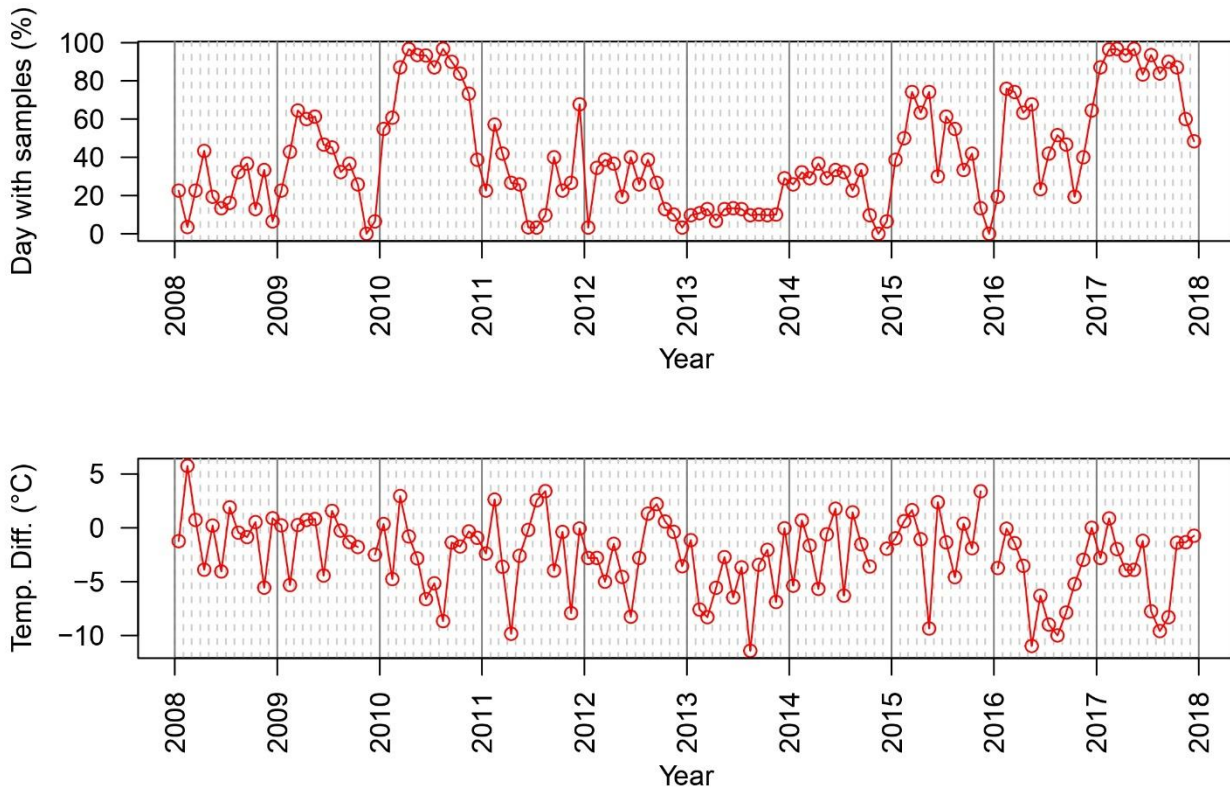
Figure S6. Time series showing the percentage of days with collected samples in a month (upper) and difference of T_{AWS} between days with collected samples and days without samples at monthly basis (bottom).
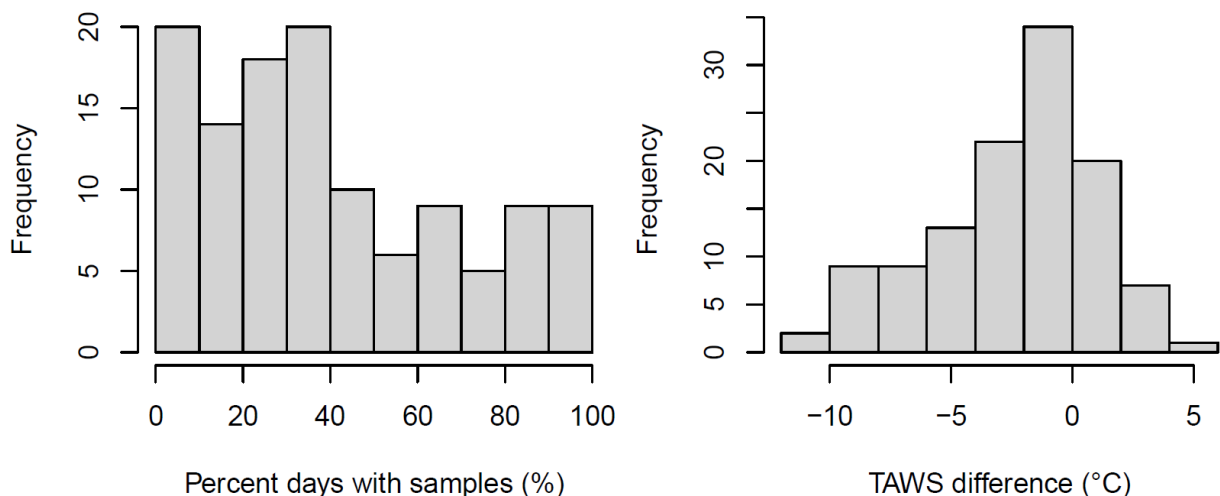
Figure S7. Histograms showing the frequency of percentage of days with collected samples in a month (upper) and difference of T_{AWS} between days with collected samples and days without samples at monthly basis (bottom).
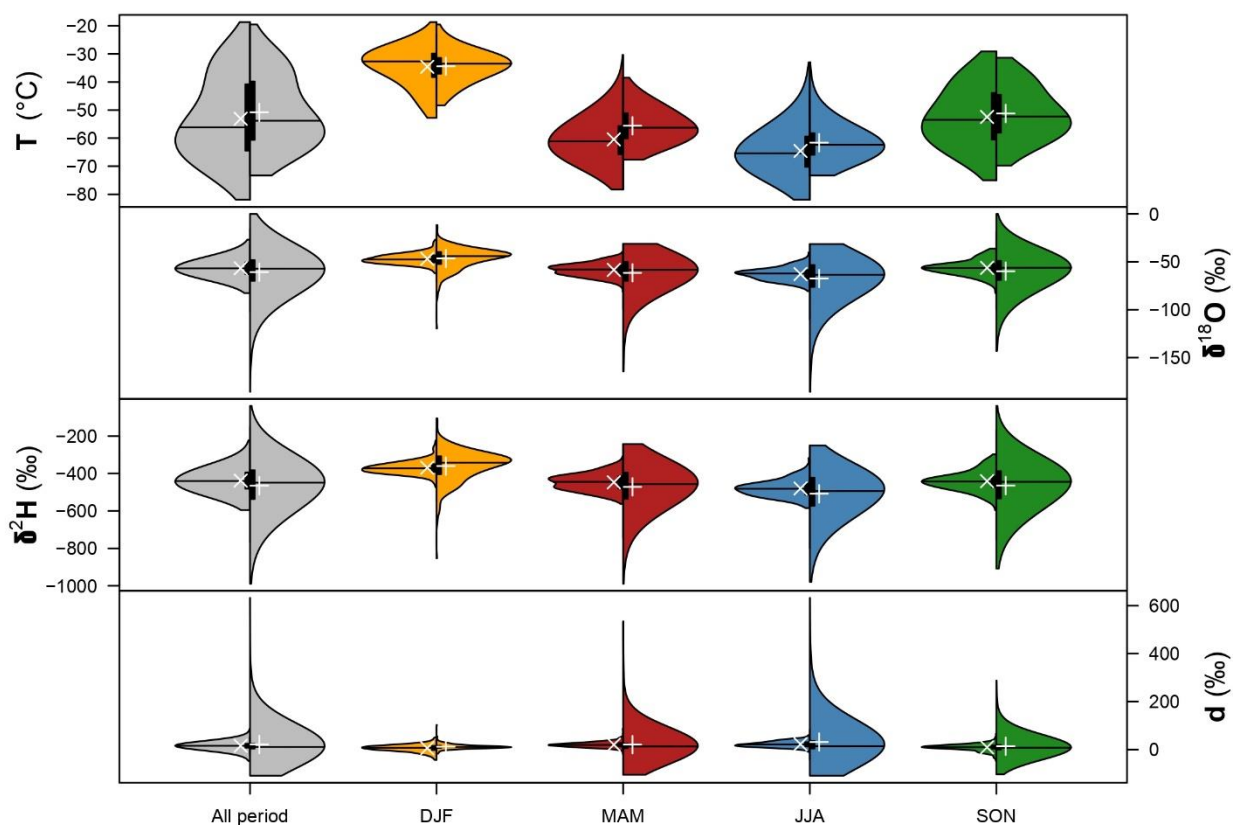
Figure S8. Violin plots of the data experimentally measured at Concordia station (left side of the plots) and modeled by ECHAM5-wiso (right side) over all the 2008-2017 period and for each season. The upper plot reports the daily-averaged air temperatures measured by AWS (T_{AWS}) against the $T_{2m\ ECHAM5}$; the remaining plots show the isotopic composition of snow. The colored areas of the violin plots show rotated kernel densities, the vertical boxes inside the violin plots refer to the interquartile range, the vertical bars to the 1.5*interquartile ranges, the white symbols represent the arithmetic means ("×" for Concordia station and "+" for ECHAM5-wiso), and the horizontal lines show the medians.
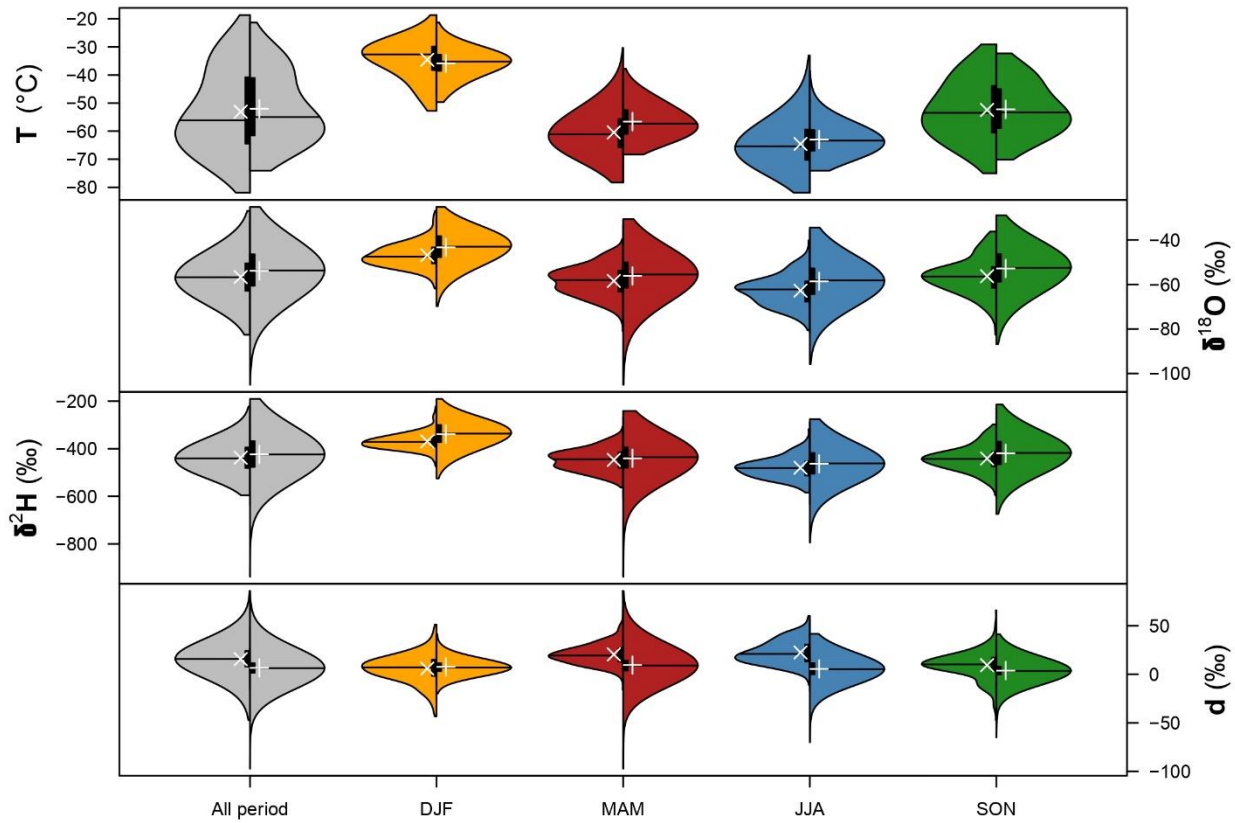
Figure S9. Violin plots of the data experimentally measured at Concordia station (left side of the plots) and modeled by ECHAM6-wiso (right side) over all the 2008-2017 period and for each season. The upper plot reports the daily-averaged air temperatures measured by AWS (T_{AWS}) against the $T_{2m\ ECHAM6}$; the remaining plots show the isotopic composition of snow. The colored areas of the violin plots show rotated kernel densities, the vertical boxes inside the violin plots refer to the interquartile range, the vertical bars to the 1.5*interquartile ranges, the white symbols represent the arithmetic means ("x" for Concordia station and "+" for ECHAM6-wiso), and the horizontal lines show the medians.
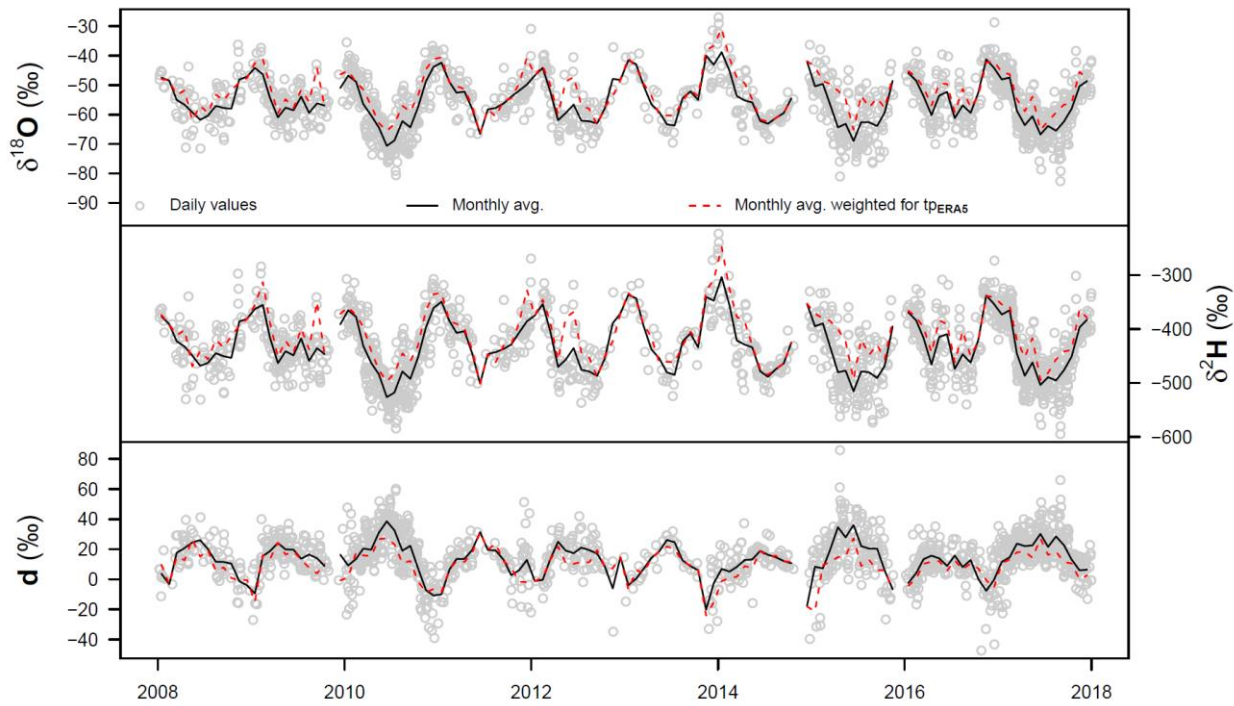
Figure S10. Time series of the daily and monthly-averaged isotopic composition of precipitation. Daily data: grey circles, monthly arithmetic means: black continuous lines, monthly averages weighted for the ERA5 tp (total precipitation): red dashed lines.
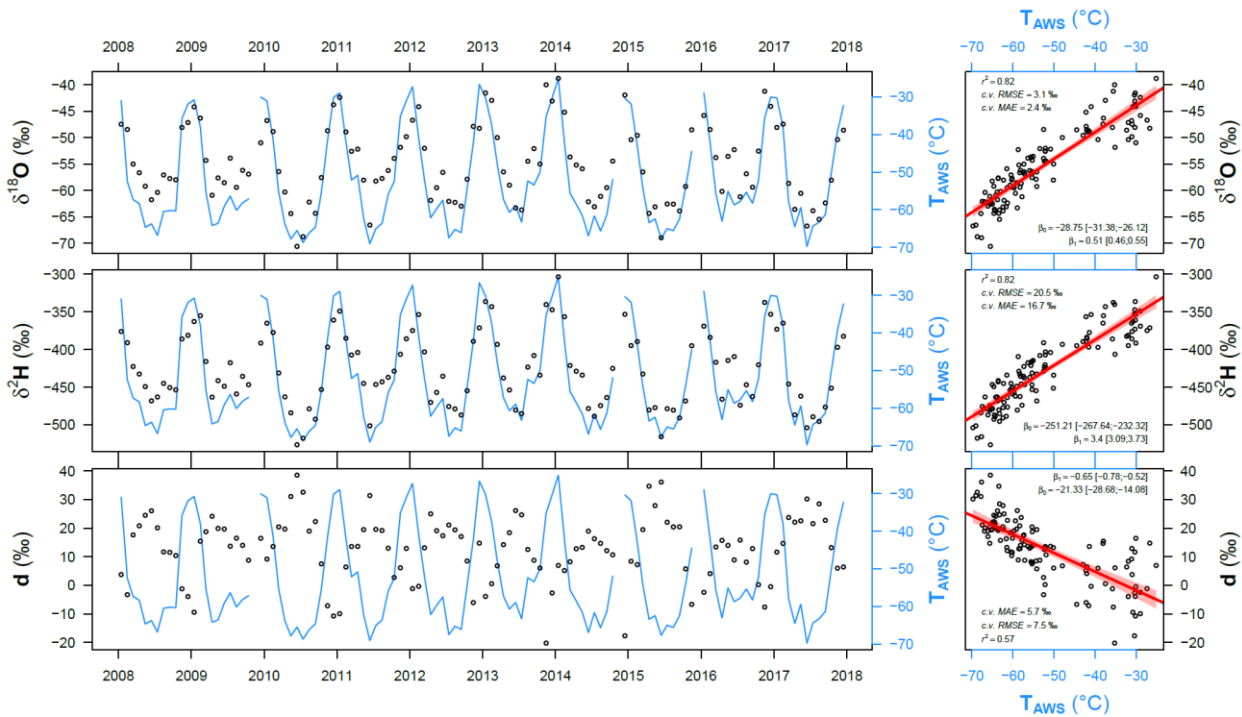
Figure SI11. Left: time series of the monthly-averaged air temperature measured by AWS (blue lines) and the isotopic composition of snow (black circles) measured at Concordia during 2008-2017. The monthly T_{AWS} were computed on the days with snow samples available. Right: linear regressions between the monthly-averaged isotopic composition of snow and T_{AWS}.
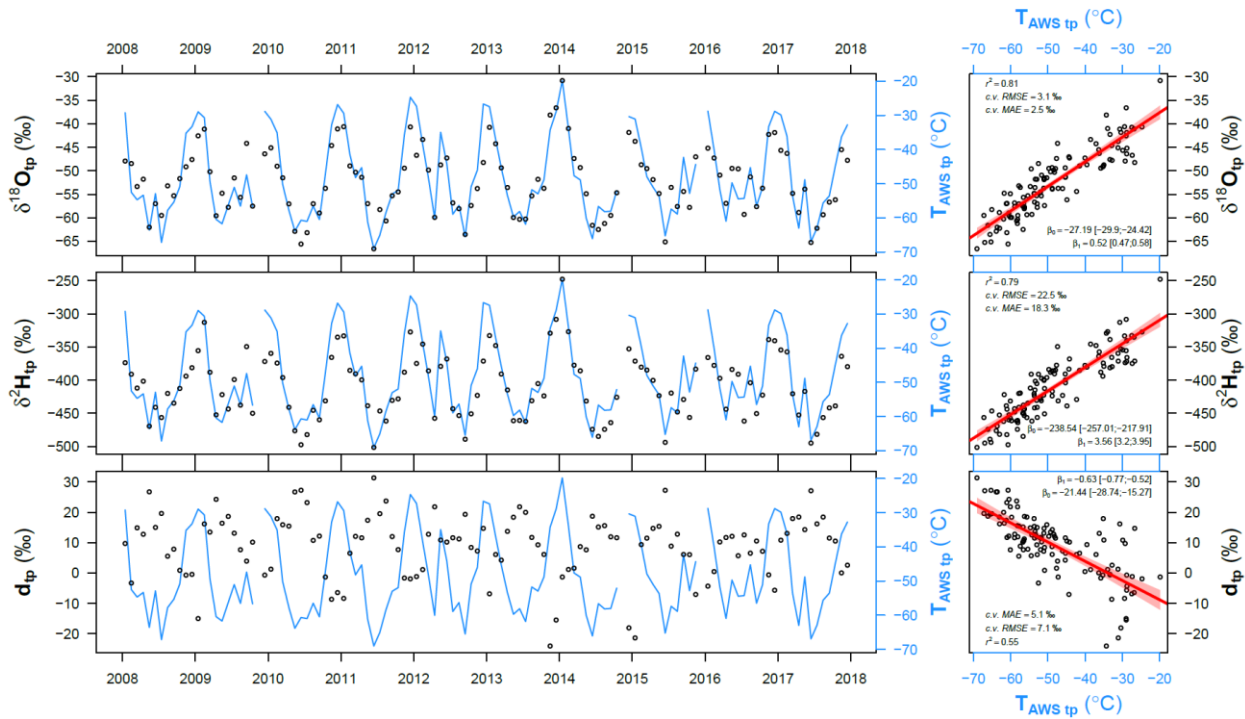
Figure S12. Left: time series of the monthly-averaged air temperature measured by AWS (blue lines) and the isotopic composition of snow (black dots), both weighted for the ERA5 total precipitation (tp). The monthly $T_{AWS\ tp}$ were computed on the days with snow samples available. **Right:** linear regressions between the monthly-averaged isotopic composition of snow and air temperature measured by AWS, both weighted for the ERA5 total precipitation.
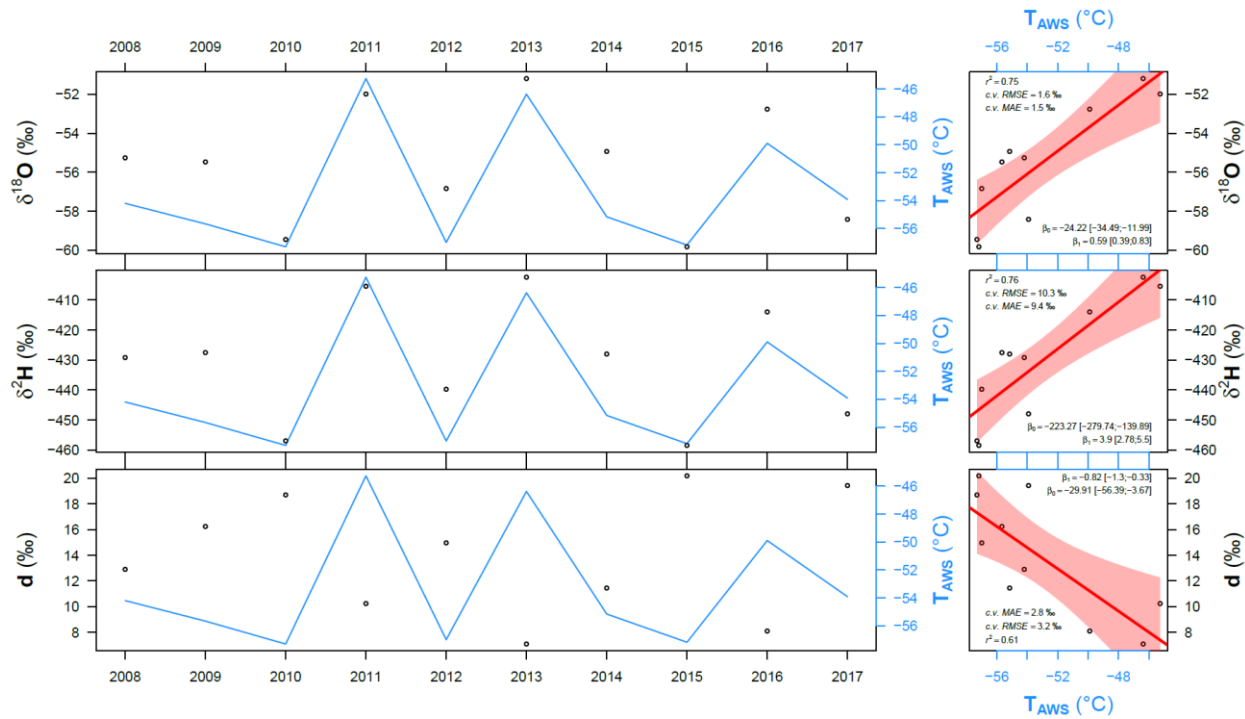
Figure S13. Left: time series of the annually-averaged air temperature measured by AWS (blue lines) and the isotopic composition of snow (black circles) measured at Concordia during 2008-2017. The annual T_{AWS} were computed on the days with snow samples available. **Right:** linear regressions between the annually-averaged isotopic composition of snow and air temperature measured by AWS.
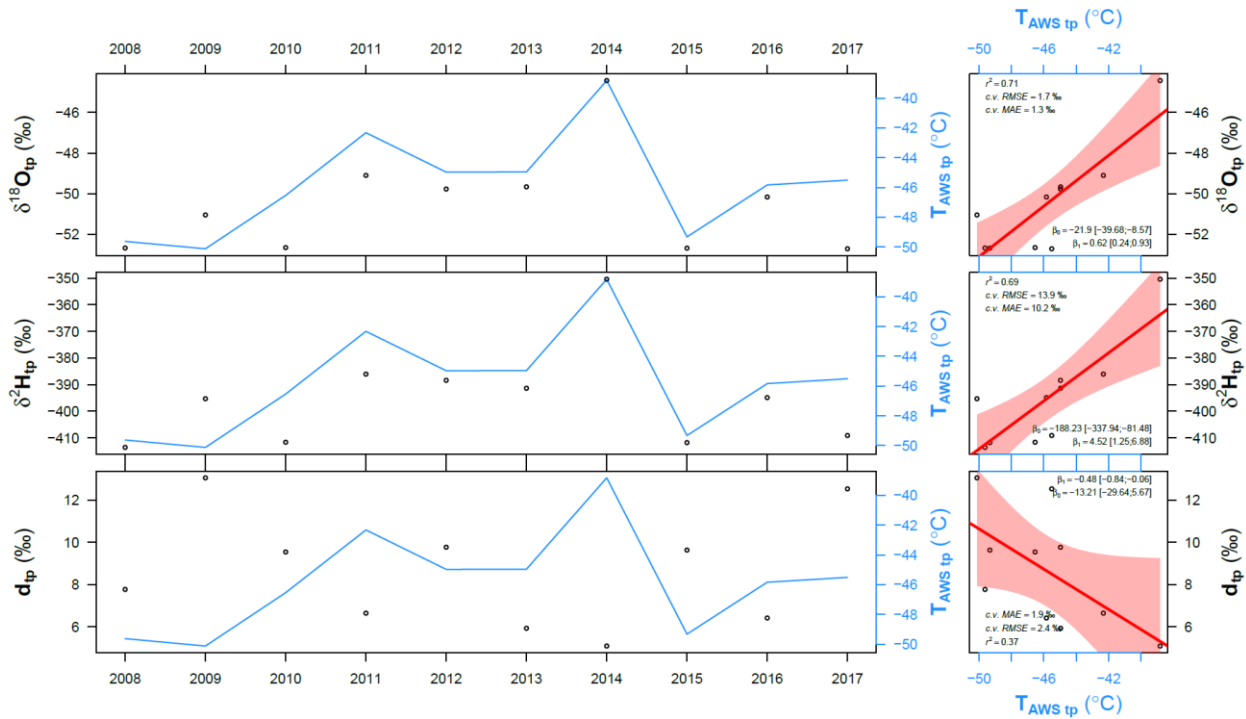
Figure S14. Left: time series of the annually-averaged air temperature measured by AWS (blue lines) and the isotopic composition of snow (black dots), both weighted for the ERA5 total precipitation (tp). The annual $T_{AWS\ tp}$ were computed on the days with snow samples available. Right: linear regressions between the annually-averaged isotopic composition of snow and air temperature measured by AWS, both weighted for the ERA5 total precipitation.
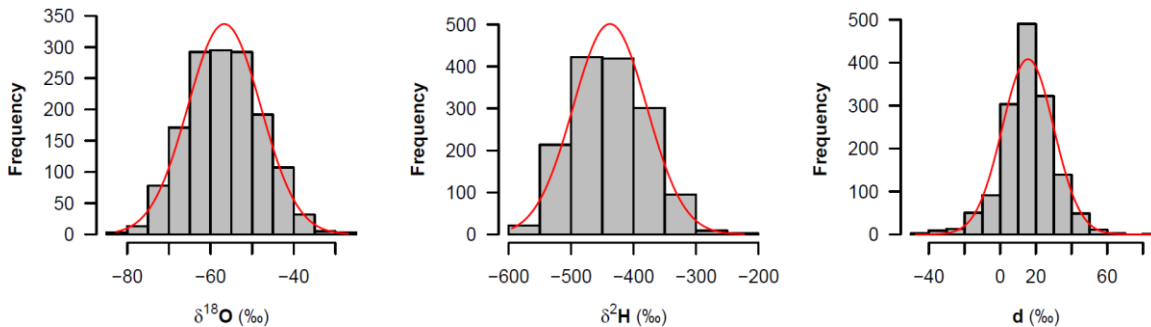
Figure S15. Histograms for the delta values and d-excess also show normal curves with the same mean and standard deviation to quickly compare the distribution of data to a normal distribution (red lines).
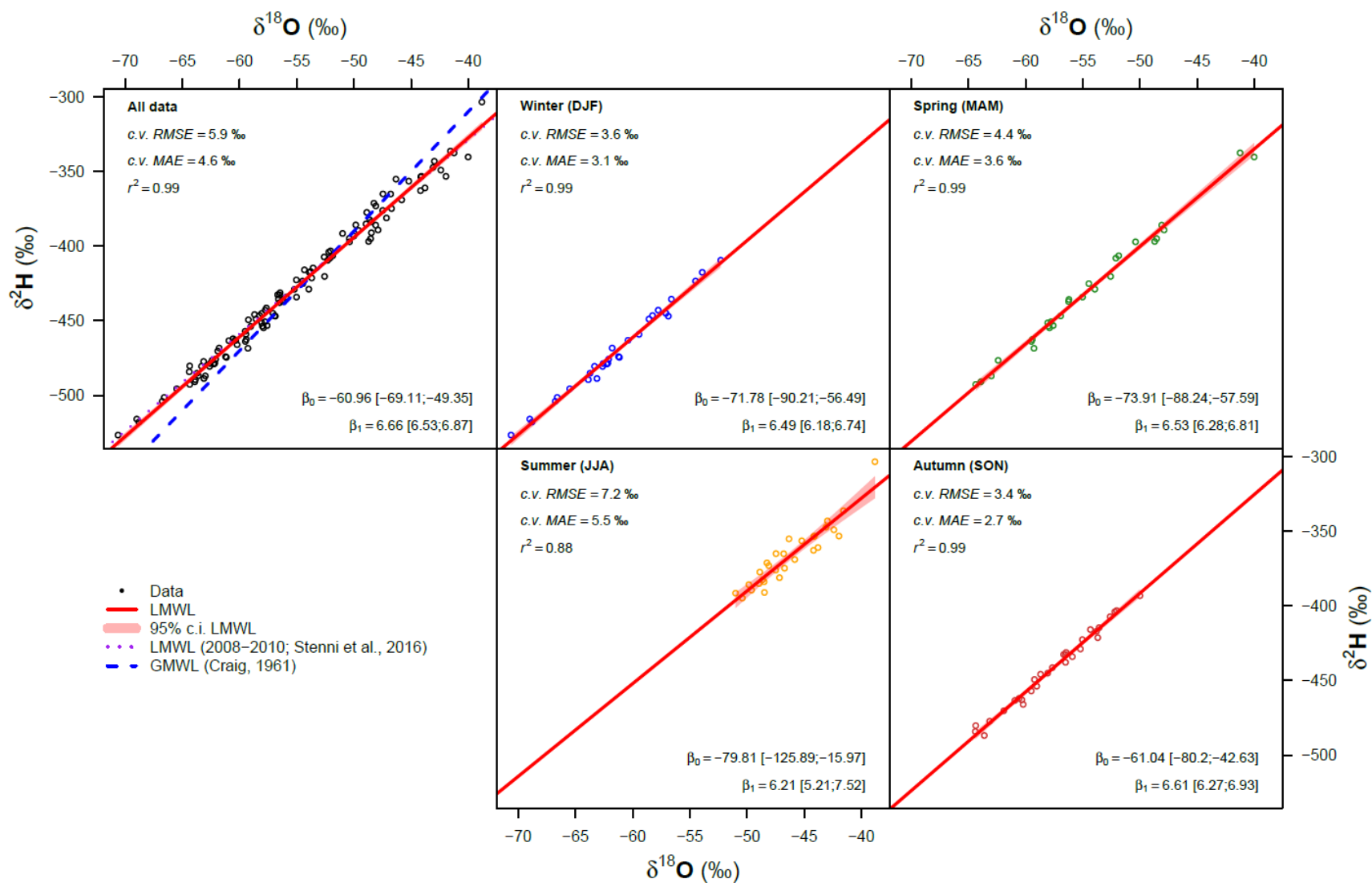
Figure S16. Local meteoric water lines computed on the monthly averaged data; the results are reported for the entire dataset (upper left) and for the single seasons. Regression parameters are also summarized in Table 2. The plot for all data also illustrates LMWLs reported by Stenni et al. (2016) and the global meteoric water line by Craig (1961).
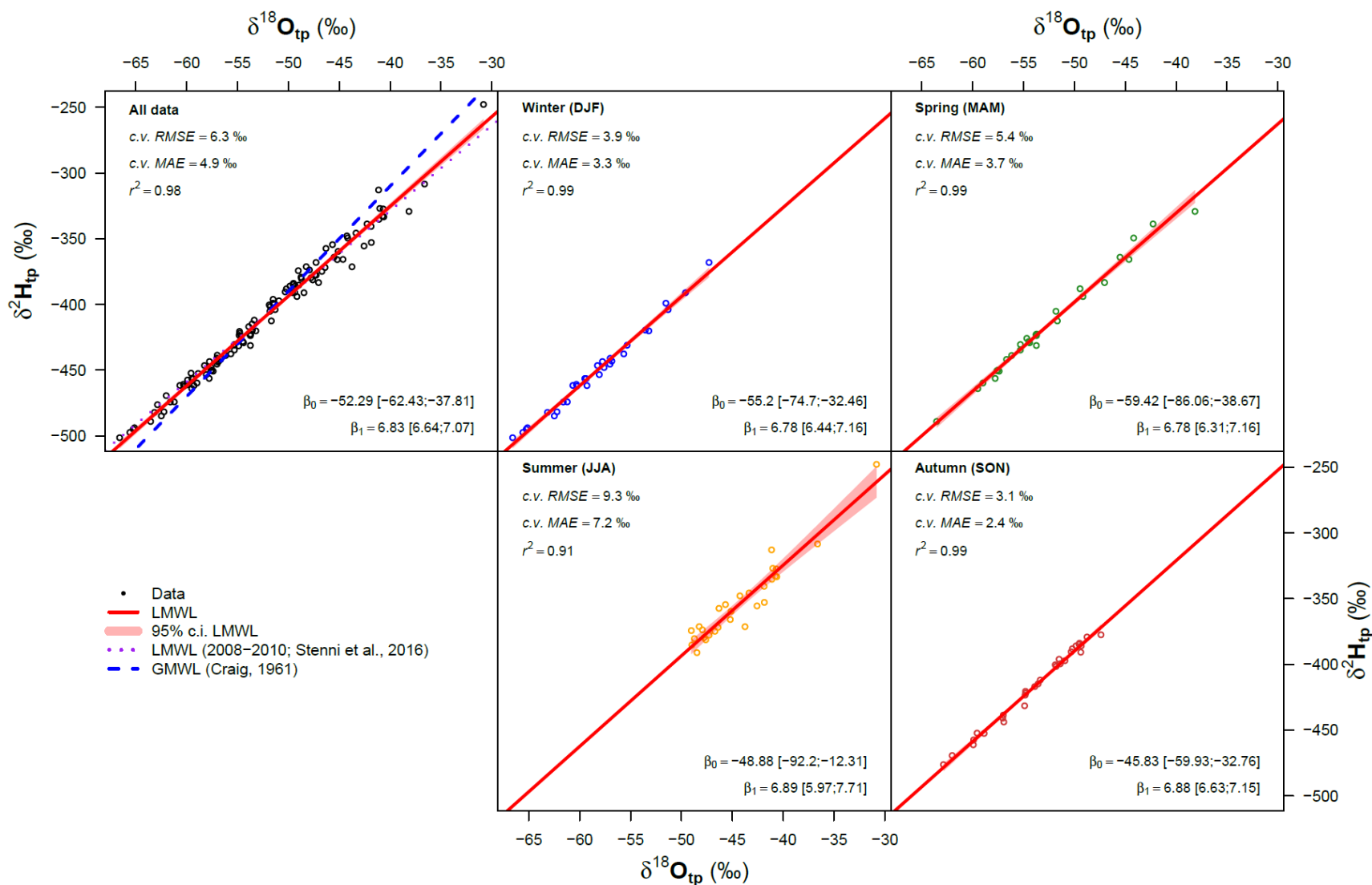
Figure S17. Local meteoric water lines computed on the monthly averaged data weighted for the ERA5 total precipitation (tp); the results are reported for the entire dataset (upper left) and for the single seasons. Regression parameters are also summarized in Table 2. The plot for all data also illustrates LMWLs reported by Stenni et al. (2016) and the global meteoric water line by Craig (1961).
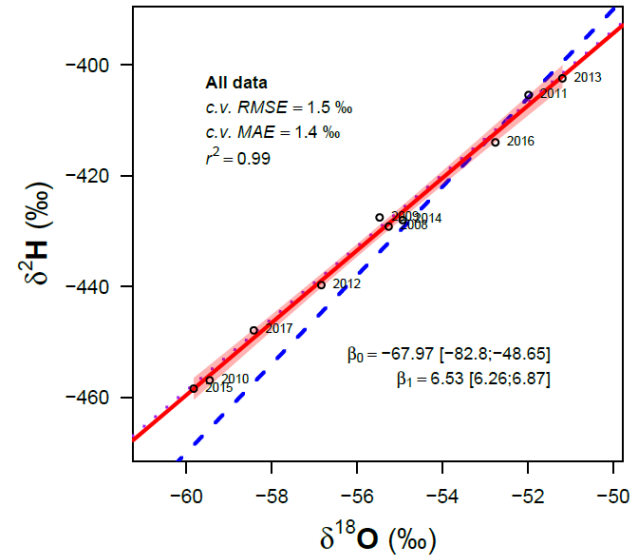
Figure S18. Local meteoric water lines computed on the annual averaged data. Regression parameters are also summarized in Table 2. The plot for all data also illustrates LMWLs reported by Stenni et al. (2016) and the global meteoric water line by Craig (1961).
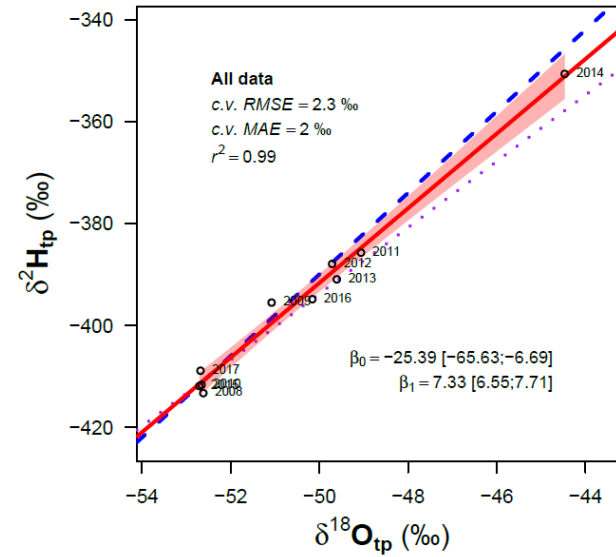
Figure S19. Local meteoric water lines computed on the annual averaged data weighted for the ERA5 total precipitation. Regression parameters are also summarized in Table 2. The plot for all data also illustrates LMWLs reported by Stenni et al. (2016) and the global meteoric water line by Craig (1961).
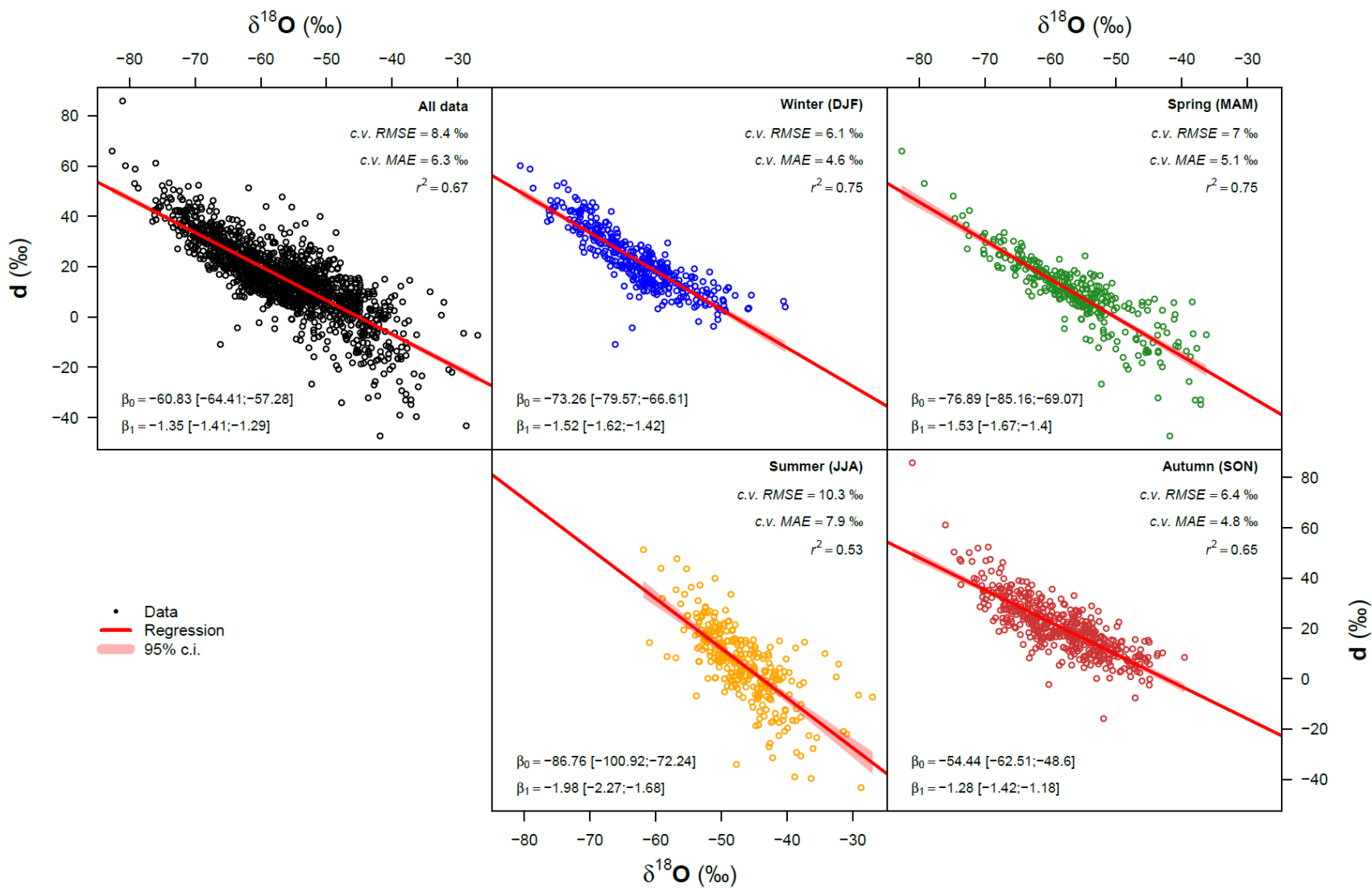
Figure S20. Linear relationships between δ^{18}O and deuterium excess computed on the daily data; the results are reported for the entire dataset (upper left) and for the single seasons. Regression parameters are also summarized in Table SI1.
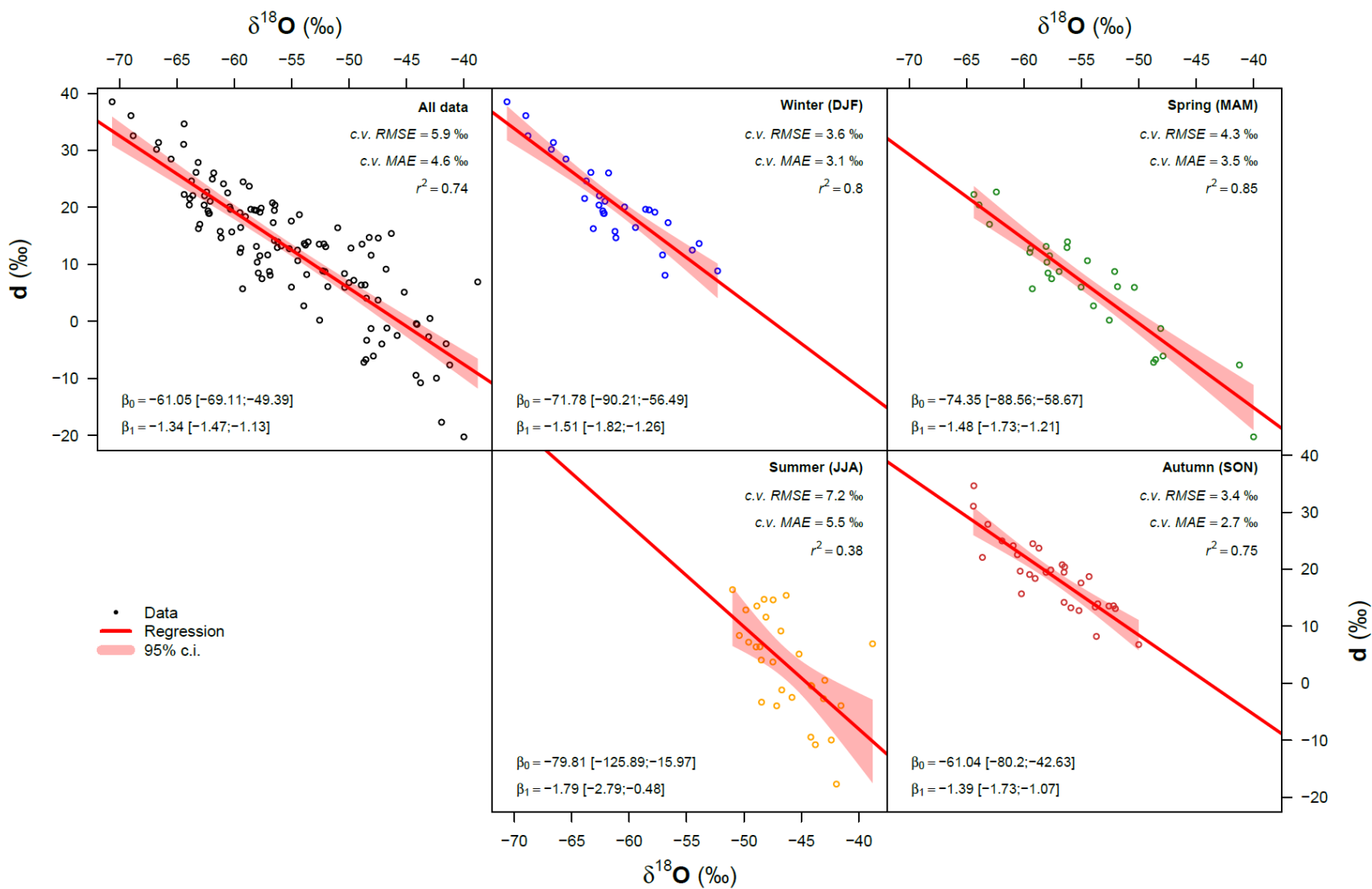
Figure S21. Linear relationships between δ¹⁸O and deuterium excess computed on the monthly-averaged data; the results are reported for the entire dataset (upper left) and for the single seasons. Regression parameters are also summarized in Table SI1.

Figure S22. Linear relationships between $\delta^{18}O$ and deuterium excess computed on the monthly-averaged data weighted for the ERA5 total precipitation (tp); the results are reported for the entire dataset (upper left) and for the single seasons. Regression parameters are also summarized in Table SI1.
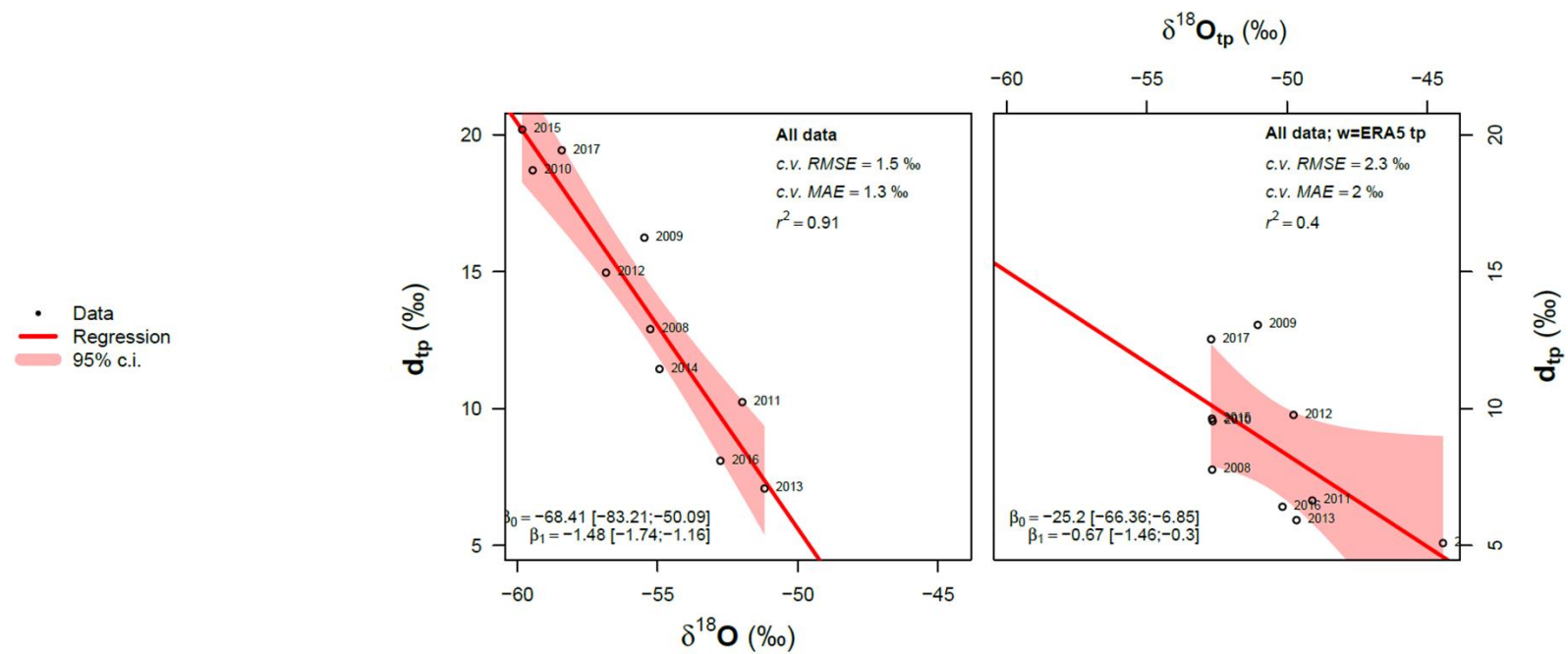
Figure S23. Linear relationships between δ¹⁸O and deuterium excess computed on the annual-averaged data (left) and on the annual-averaged data weighted for the ERA5 total precipitation (tp) (right). Regression parameters are also summarized in Table SI1.
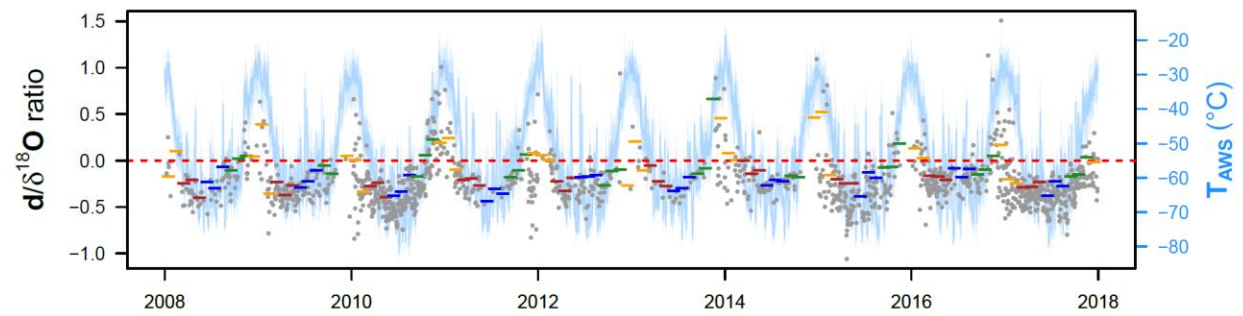
Figure S24. Daily d-excess to δ¹⁸O ratio (grey dots) against the air temperature (blue line). The monthly d/δ¹⁸O ratios are also shown (bars: gold=Austral summer, red= autumn, blue=winter, green=spring).
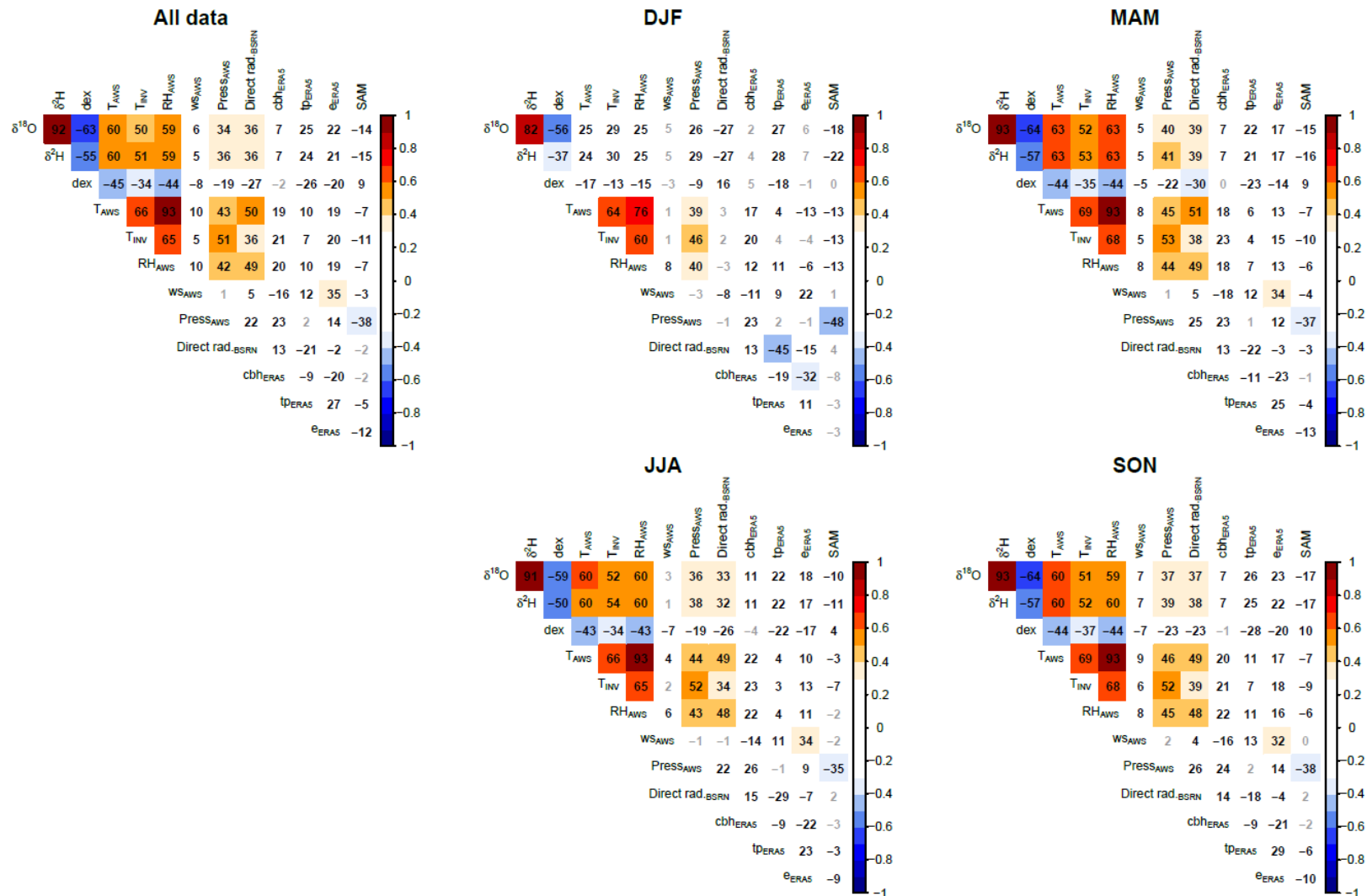
Figure S25. Kendall's correlation matrixes computed on the daily data. The results are reported for the entire dataset (upper left) and for each season. Correlations are reported as percentage (-100 to +100) to save space; correlations not significant (p>0.05) are in grey.
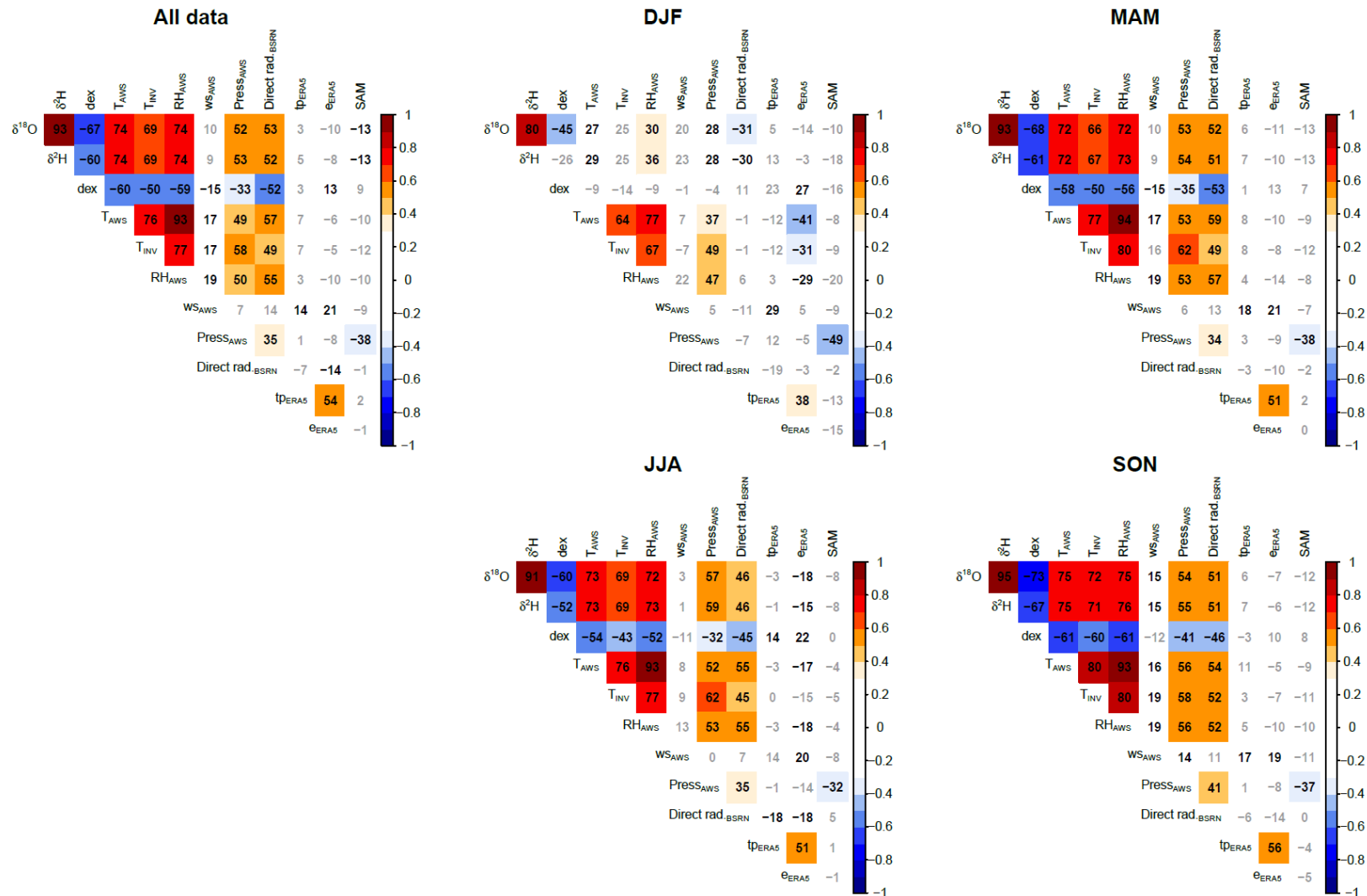
Figure S26. Kendall's correlation matrixes computed on the monthly averaged data. The results are reported for the entire dataset (upper left) and for each season. Correlations are reported as percentage (-100 to +100) to save space; correlations not significant (p>0.05) are in grey.
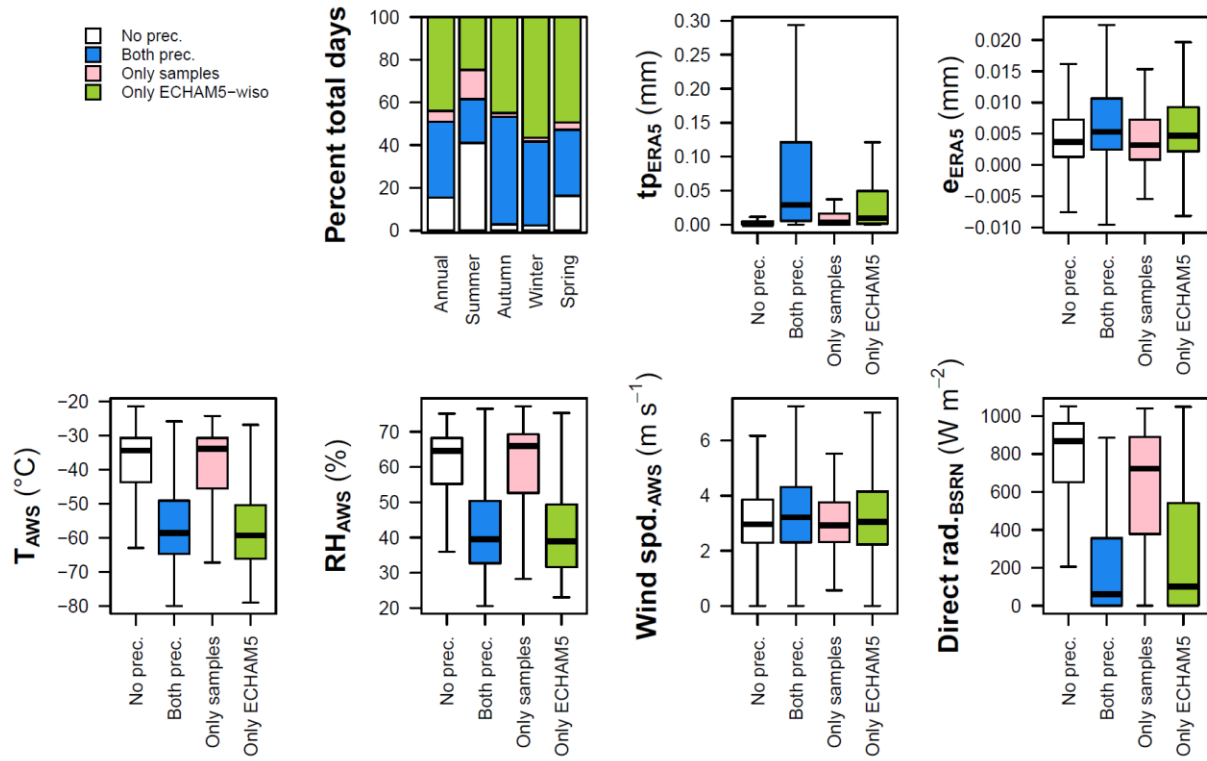
Figure S27. Statistics on the days with agreement or disagreement between ECHAM5-wiso and the experimental observations.
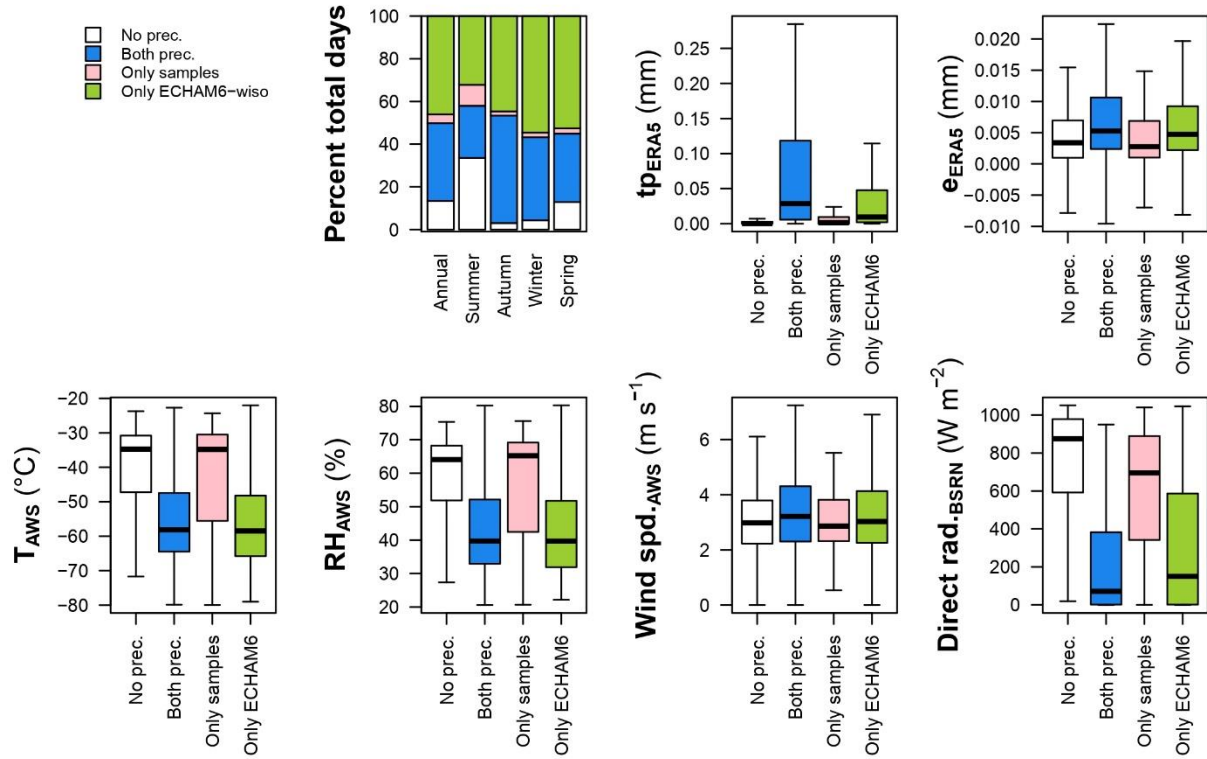
Figure S28. Statistics on the days with agreement or disagreement between ECHAM6-wiso and the experimental observations.
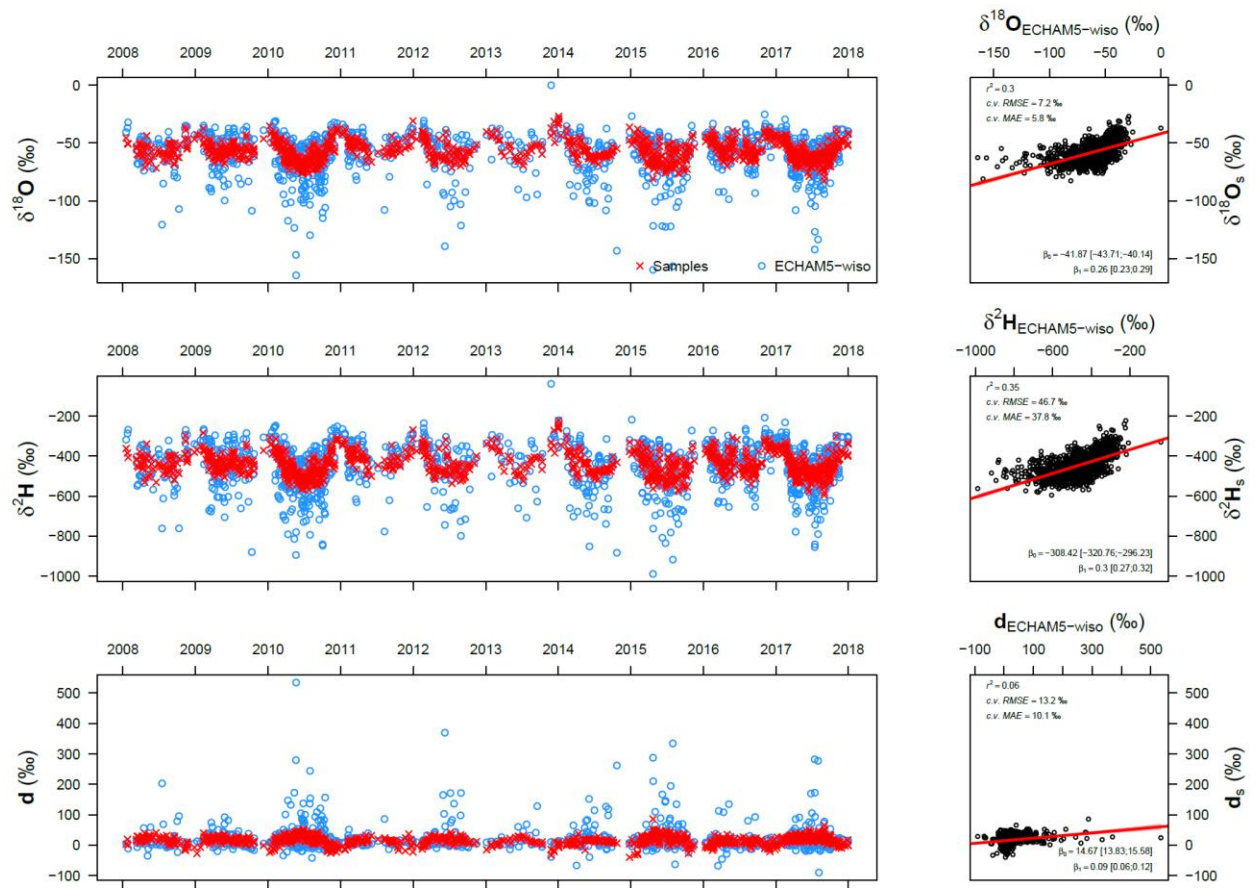
Figure S29. Time series of the delta values analyzed experimentally (red crosses) and modeled by the ECHAM5-wiso model (blue circles) and their linear regressions.
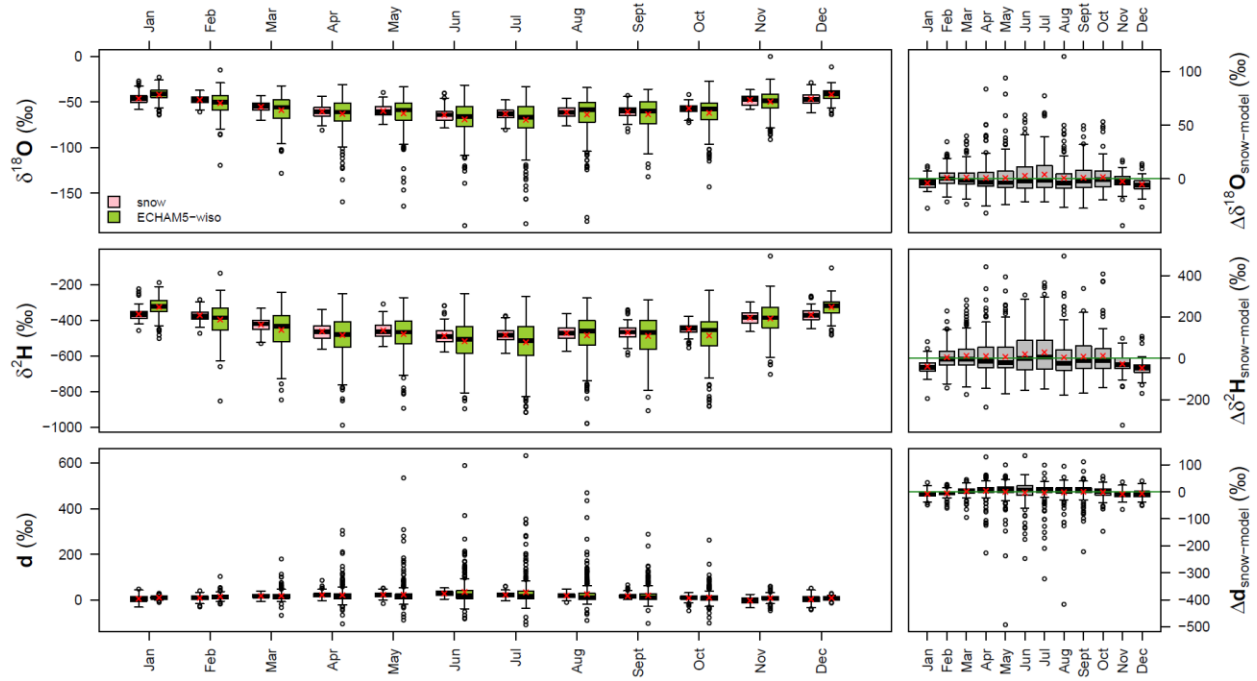
Figure S30. Seasonal variation of the experimentally measured data and ECHAM5-wiso models (left) and their difference (right); line = median, box = inter-quartile range, whiskers = ±1.5*inter-quartile range, circles = outliers and extremes; red crosses = arithmetic mean.
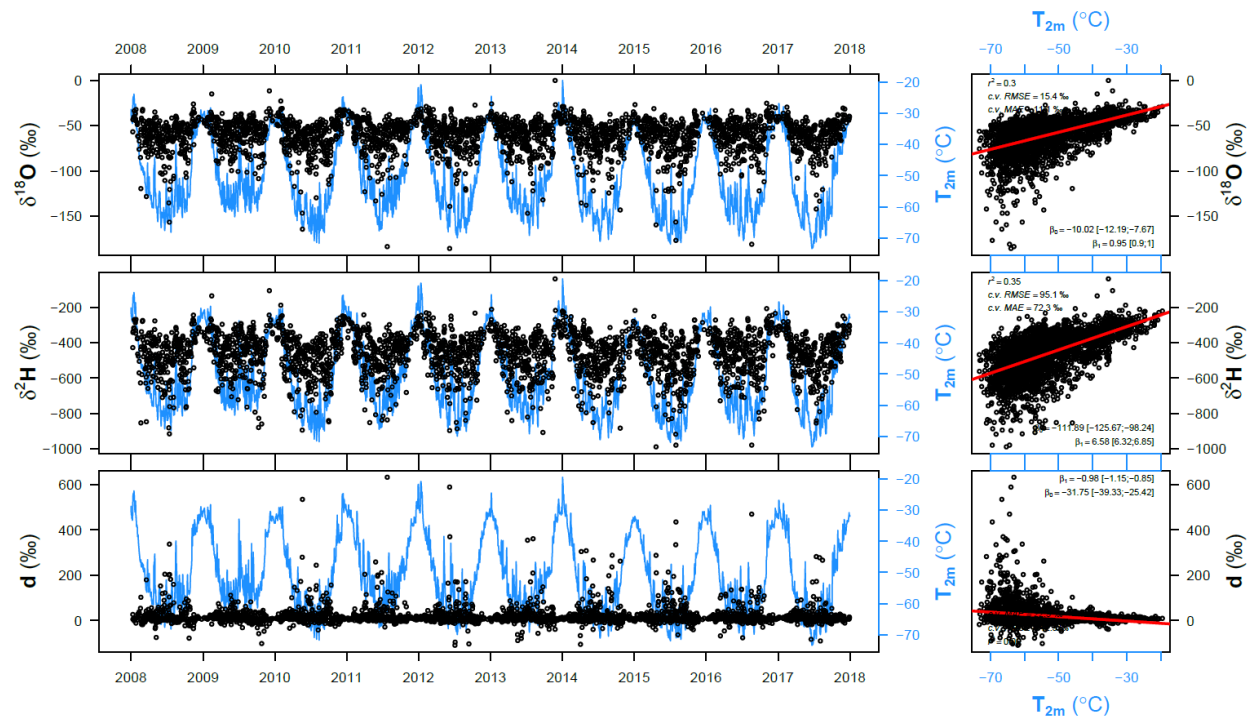
Figure S31. Left: time series of the daily-averaged air temperature (blue lines) and the isotopic composition of snow (black dots) modeled by ECHAM5-wiso. Right: linear regressions between the isotopic composition of precipitation and air temperature modeled by ECHAM5-wiso.
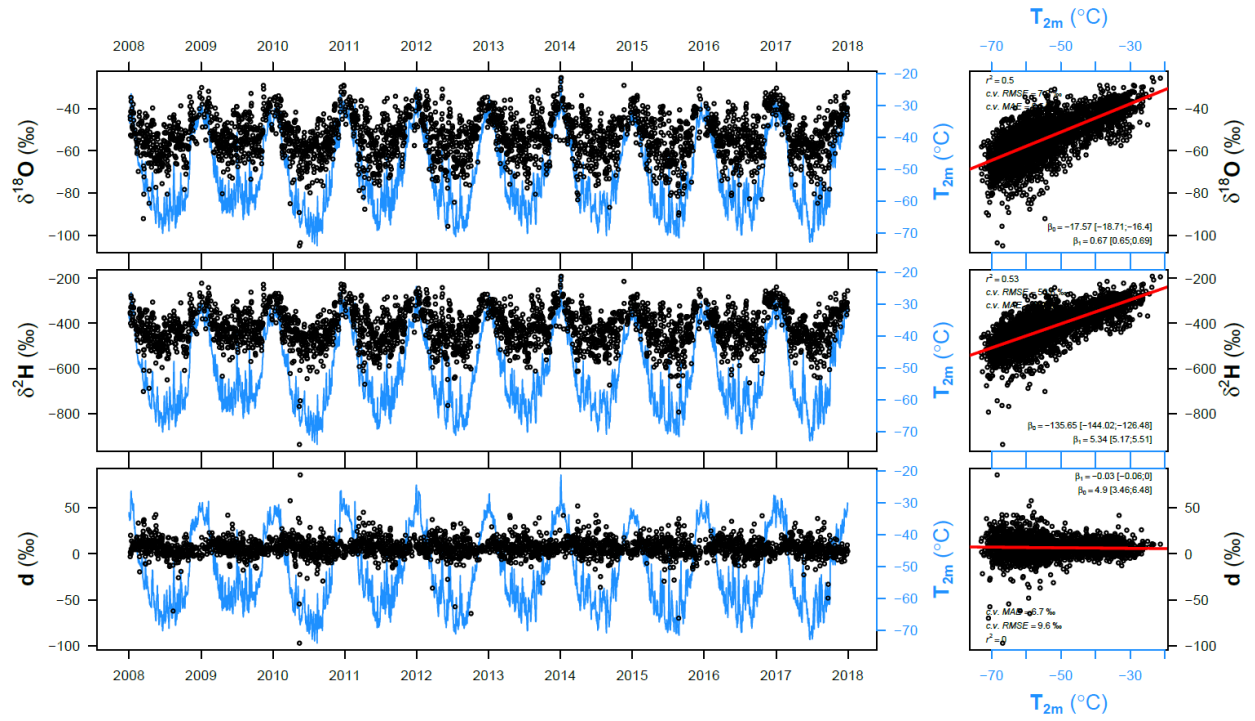
Figure S32. Left: time series of the daily averaged air temperature (blue lines) and the isotopic composition of snow (black dots) modelized by ECHAM6-wiso. Right: linear regressions between the isotopic composition of precipitation and air temperature modeled by ECHAM6-wiso.
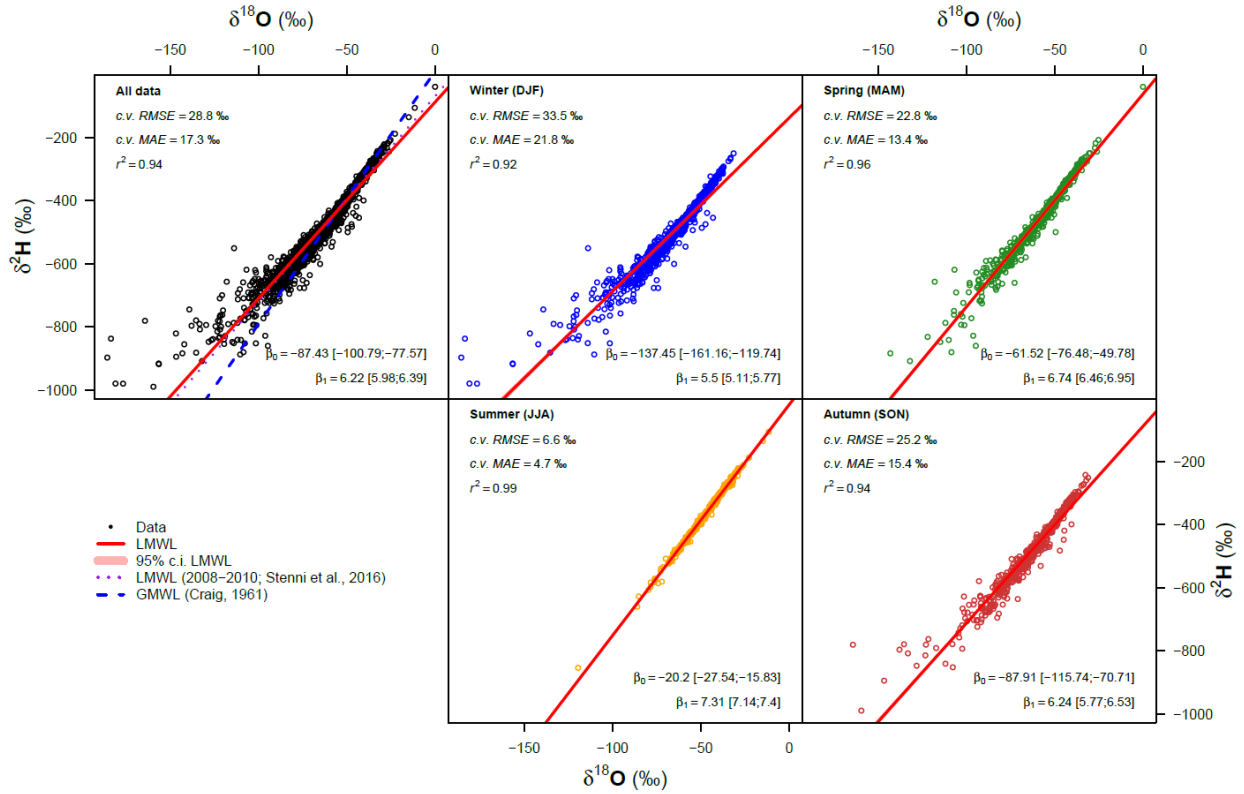
Figure S33. Local meteoric water lines computed on the isotopic composition of the daily samples by using ECHM5-wiso outputs. Regression parameters are also summarized in Table SI3. The plot for all data also illustrates LMWLs reported by Stenni et al. (2016) and the global meteoric water line by Craig (1961).
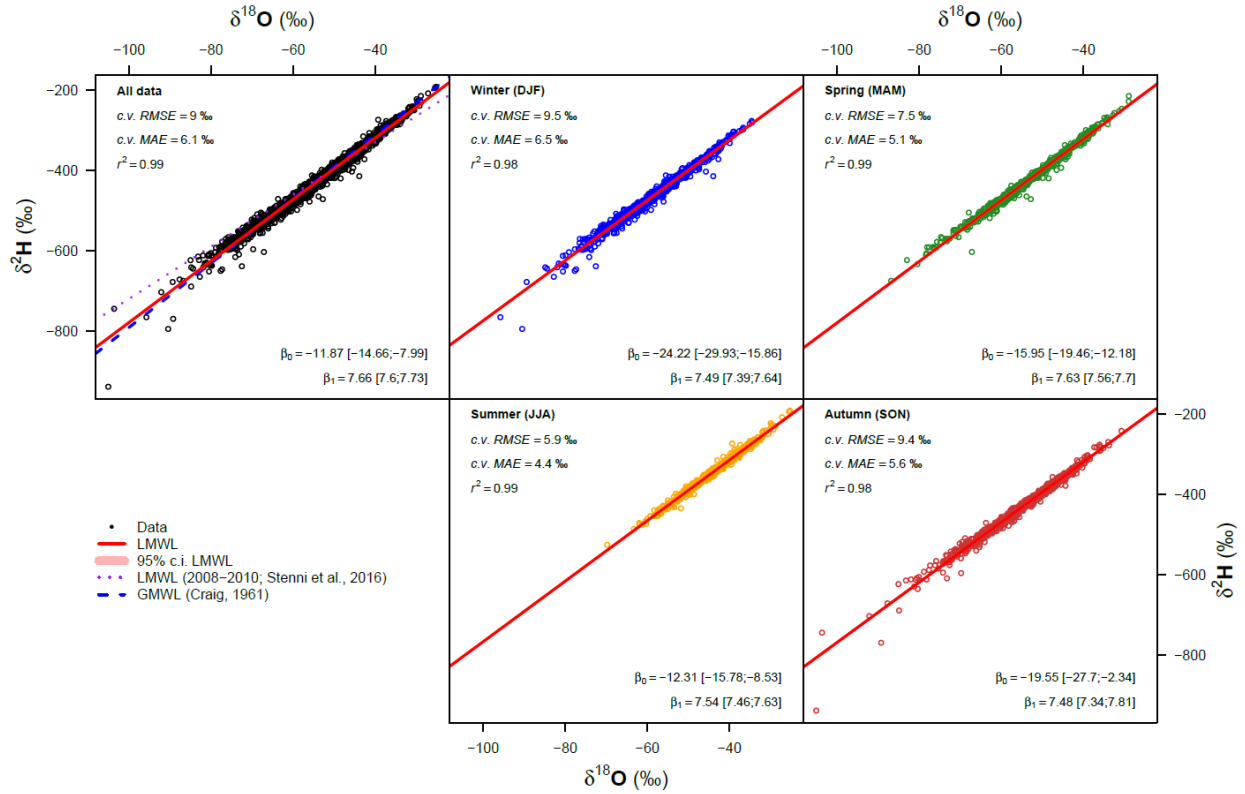
Figure S34. Local meteoric water lines computed on the isotopic composition of the daily samples by using ECHM6-wiso outputs. Regression parameters are also summarized in Table SI3. The plot for all data also illustrates LMWLs reported by Stenni et al. (2016) and the global meteoric water line by Craig (1961).

Table S1. Relationships between $\delta^{18}O$ and d-excess.

Regression variables		Data used	Intercept		Slope		r^2	CV RMSE
Dependent	Indipendent		β_0 (±std. error)	BS 95th CI	β_1 (±std. error)	BS 95th CI		‰
d	$\delta^{18}O$	Daily, all data	-61 (±1)	[-64;-57]	-1.35 (±0.02)	[-1.41;-1.29]	0.67	8.4
d	$\delta^{18}O$	Daily, winter (JJA)	-73 (±3)	[-80;-67]	-1.52 (±0.05)	[-1.62;-1.42]	0.75	6.1
d	$\delta^{18}O$	Daily, spring (SON)	-77 (±3)	[-85;-69]	-1.53 (±0.05)	[-1.67;-1.4]	0.75	7
d	$\delta^{18}O$	Daily, summer (DJF)	-87 (±5)	[-101;-72]	-1.98 (±0.11)	[-2.27;-1.68]	0.53	10.3
d	$\delta^{18}O$	Daily, autumn (MAM)	-54 (±3)	[-63;-49]	-1.28 (±0.04)	[-1.42;-1.18]	0.65	6.4
d	$\delta^{18}O$	Monthly, all data	-61 (±4)	[-69;-49]	-1.34 (±0.07)	[-1.47;-1.13]	0.74	5.9
d	$\delta^{18}O$	Monthly, winter (JJA)	-72 (±9)	[-90;-56]	-1.51 (±0.14)	[-1.82;-1.26]	0.80	3.6
d	$\delta^{18}O$	Monthly, spring (SON)	-74 (±7)	[-89;-59]	-1.48 (±0.12)	[-1.73;-1.21]	0.85	4.3
d	$\delta^{18}O$	Monthly, summer (DJF)	-80 (±21)	[-126;-16]	-1.79 (±0.44)	[-2.79;-0.48]	0.38	7.2
d	$\delta^{18}O$	Monthly, autumn (MAM)	-61 (±9)	[-80;-43]	-1.39 (±0.15)	[-1.73;-1.07]	0.75	3.4
d_{tp}	$\delta^{18}O_{tp}$	Weighted monthly, all data	-53 (±4)	[-63;-39]	-1.18 (±0.08)	[-1.36;-0.93]	0.64	6.3
d_{tp}	$\delta^{18}O_{tp}$	Weighted monthly, winter (JJA)	-55 (±8)	[-75;-32]	-1.22 (±0.14)	[-1.56;-0.84]	0.72	3.9
d_{tp}	$\delta^{18}O_{tp}$	Weighted monthly, spring (SON)	-62 (±8)	[-84;-40]	-1.26 (±0.14)	[-1.68;-0.88]	0.75	5.1
d_{tp}	$\delta^{18}O_{tp}$	Weighted monthly, summer (DJF)	-49 (±18)	[-92;-12]	-1.11 (±0.41)	[-2.03;-0.29]	0.21	9.3
d_{tp}	$\delta^{18}O_{tp}$	Weighted monthly, autumn (MAM)	-46 (±7)	[-60;-33]	-1.12 (±0.14)	[-1.37;-0.85]	0.71	3.1
d	$\delta^{18}O$	Annual	-68 (±9)	[-83;-50]	-1.48 (±0.16)	[-1.74;-1.16]	0.91	1.5
d_{tp}	$\delta^{18}O_{tp}$	Weighted annual	-25 (±15)	[-66;-7]	-0.67 (±0.29)	[-1.46;-0.3]	0.40	2.3

Table S2. Results of the regressions of delta values against air temperature modeled by ECHAM5-wiso.

| Regression variables | | Data used | Intercept | | Slope | | r^2 | CV RMSE |
Dependent	Indipendent		β_0 (±std. error)	BS 95th CI	β_1 (±std. error)	BS 95th CI		‰
$\delta^{18}O$	T_{2m}	Daily, all data	-10 (±1)	[-12;-8]	0.95 (±0.03)	[0.9;1]	0.30	15.44
δ^2H	T_{2m}	Daily, all data	-112 (±9)	[-126;-98]	6.58 (±0.17)	[6.32;6.85]	0.35	95.1
d	T_{2m}	Daily, all data	-32 (±4)	[-39;-25]	-0.98 (±0.07)	[-1.15;-0.85]	0.06	42.3
$\delta^{18}O$	T_{2m}	Monthly, all data	-17 (±2)	[-20;-14]	0.82 (±0.03)	[0.76;0.88]	0.85	4.06
δ^2H	T_{2m}	Monthly, all data	-148 (±11)	[-168;-128]	5.9 (±0.21)	[5.51;6.31]	0.87	27.7
d	T_{2m}	Monthly, all data	-14 (±4)	[-21;-8]	-0.65 (±0.08)	[-0.8;-0.51]	0.37	10
$\delta^{18}O_{prec}$	$T_{2m\ prec}$	Weighted monthly, all data	-23 (±1)	[-25;-20]	0.53 (±0.03)	[-25.47;-20.45]	0.77	3.21
δ^2H_{prec}	$T_{2m\ prec}$	Weighted monthly, all data	-178 (±10)	[-196;-159]	4.17 (±0.2)	[-195.93;-158.65]	0.79	24.1
d_{prec}	$T_{2m\ prec}$	Weighted monthly, all data	6 (±2)	[3;9]	-0.07 (±0.04)	[2.61;9.35]	0.03	4.3
$\delta^{18}O$	T_{2m}	Annual, all data	-29 (±14)	[-62;-2]	0.59 (±0.26)	[-0.03;1.08]	0.40	1.6
δ^2H	T_{2m}	Annual, all data	-250 (±82)	[-439;-106]	4.01 (±1.52)	[0.39;6.54]	0.47	10
d	T_{2m}	Annual, all data	-17 (±37)	[-97;82]	-0.71 (±0.69)	[-2.15;1.15]	0.12	4.4
$\delta^{18}O_{prec}$	$T_{2m\ prec}$	Weighted annual, all data	-36 (±5)	[-47;-23]	0.23 (±0.1)	[-47.33;-22.98]	0.40	1
δ^2H_{prec}	$T_{2m\ prec}$	Weighted annual, all data	-275 (±38)	[-359;-162]	1.94 (±0.81)	[-358.79;-162.29]	0.42	8.5
d_{prec}	$T_{2m\ prec}$	Weighted annual, all data	15 (±5)	[6;27]	0.12 (±0.11)	[6.2;27.24]	0.13	1.2

Table S3. Local meteoric water lines (LMWLs) computed over different time periods using ECHAM5-wiso outputs.

Regression variables		Data used	Intercept		Slope		r^2	CV RMSE
Dependent	Indipendent		β_0 (±std. error)	BS 95th CI	β_1 (±std. error)	BS 95th CI		‰
δ^2H	$\delta^{18}O$	Daily, all data	-87 (±2)	[-101;-78]	6.22 (±0.03)	[5.98;6.39]	0.94	28.8
δ^2H	$\delta^{18}O$	Daily, winter (JJA)	-137 (±4)	[-161;-120]	5.5 (±0.05)	[5.11;5.77]	0.92	33.5
δ^2H	$\delta^{18}O$	Daily, spring (SON)	-62 (±3)	[-76;-50]	6.74 (±0.05)	[6.46;6.95]	0.96	22.8
δ^2H	$\delta^{18}O$	Daily, summer (DJF)	-20 (±1)	[-28;-16]	7.31 (±0.03)	[7.14;7.4]	0.99	6.6
δ^2H	$\delta^{18}O$	Daily, autumn (MAM)	-88 (±3)	[-116;-71]	6.24 (±0.05)	[5.77;6.53]	0.94	25.2
δ^2H	$\delta^{18}O$	Monthly, all data	-33 (±4)	[-42;-25]	7.1 (±0.07)	[6.95;7.25]	0.99	8.4
δ^2H	$\delta^{18}O$	Monthly, winter (JJA)	-91 (±16)	[-118;-64]	6.19 (±0.23)	[5.79;6.57]	0.96	8.1
δ^2H	$\delta^{18}O$	Monthly, spring (SON)	-31 (±10)	[-53;-9]	7.25 (±0.17)	[6.86;7.68]	0.98	7.7
δ^2H	$\delta^{18}O$	Monthly, summer (DJF)	-12 (±3)	[-19;-5]	7.49 (±0.07)	[7.34;7.63]	1.00	2.4
δ^2H	$\delta^{18}O$	Monthly, autumn (MAM)	-79 (±18)	[-119;-29]	6.37 (±0.28)	[5.7;7.21]	0.95	5.9
δ^2H_{prec}	$\delta^{18}O_{prec}$	Weighted monthly, all data	-2 (±3)	[-7;4]	7.76 (±0.06)	[7.65;7.88]	0.99	4.1
δ^2H_{prec}	$\delta^{18}O_{prec}$	Weighted monthly, winter (JJA)	-21 (±8)	[-34;-7]	7.39 (±0.15)	[7.15;7.65]	0.99	4.5
δ^2H_{prec}	$\delta^{18}O_{prec}$	Weighted monthly, spring (SON)	-6 (±5)	[-19;2]	7.77 (±0.09)	[7.52;7.93]	1.00	2.7
δ^2H_{prec}	$\delta^{18}O_{prec}$	Weighted monthly, summer (DJF)	-3 (±7)	[-16;11]	7.69 (±0.17)	[7.36;8.06]	0.99	3.5
δ^2H_{prec}	$\delta^{18}O_{prec}$	Weighted monthly, autumn (MAM)	-8 (±6)	[-21;6]	7.63 (±0.12)	[7.37;7.89]	0.99	2.6
δ^2H	$\delta^{18}O$	Annual	-90 (±27)	[-139;-39]	6.17 (±0.45)	[5.35;6.98]	0.96	2.4
δ^2H_{prec}	$\delta^{18}O_{prec}$	Weighted annual	21 (±15)	[-1;60]	8.26 (±0.33)	[7.81;9.14]	0.99	1.2

Table S4. Results of the regressions of delta values against air temperature modeled by ECHAM6-wiso.

Regression variables		Data used	Intercept		Slope		r^2	CV RMSE
Dependent	Indipendent		β_0 (±std. error)	BS 95th CI	β_1 (±std. error)	BS 95th CI		‰
$\delta^{18}O$	T_{2m}	Daily, all data	-18 (±1)	[-19;-16]	0.67 (±0.01)	[0.65;0.69]	0.50	7.23
δ^2H	T_{2m}	Daily, all data	-136 (±5)	[-144;-126]	5.34 (±0.09)	[5.17;5.51]	0.53	53.8
d	T_{2m}	Daily, all data	5 (±1)	[3;6]	-0.03 (±0.02)	[-0.06;0]	0.00	9.6
$\delta^{18}O$	T_{2m}	Monthly, all data	-21 (±1)	[-23;-19]	0.61 (±0.02)	[0.57;0.65]	0.88	2.56
δ^2H	T_{2m}	Monthly, all data	-160 (±8)	[-176;-144]	4.87 (±0.15)	[4.6;5.17]	0.90	19
d	T_{2m}	Monthly, all data	7 (±1)	[5;10]	0.01 (±0.03)	[-0.03;0.07]	0.00	3.5
$\delta^{18}O_{prec}$	$T_{2m\ prec}$	Weighted monthly, all data	-22 (±1)	[-25;-20]	0.5 (±0.02)	[-24.64;-20.14]	0.79	2.79
δ^2H_{prec}	$T_{2m\ prec}$	Weighted monthly, all data	-169 (±9)	[-186;-151]	4.13 (±0.18)	[-186.4;-151.31]	0.81	21.7
d_{prec}	$T_{2m\ prec}$	Weighted monthly, all data	11 (±2)	[7;14]	0.11 (±0.03)	[7.48;13.71]	0.11	3.7
$\delta^{18}O$	T_{2m}	Annual, all data	-7 (±8)	[-31;7]	0.87 (±0.15)	[0.43;1.13]	0.80	0.6
δ^2H	T_{2m}	Annual, all data	-26 (±61)	[-196;83]	7.36 (±1.12)	[4.22;9.36]	0.84	4.4
d	T_{2m}	Annual, all data	30 (±12)	[10;44]	0.44 (±0.21)	[0.07;0.69]	0.34	0.7
$\delta^{18}O_{prec}$	$T_{2m\ prec}$	Weighted annual, all data	-33 (±8)	[-45;-11]	0.28 (±0.15)	[-45.2;-10.54]	0.29	1
δ^2H_{prec}	$T_{2m\ prec}$	Weighted annual, all data	-240 (±63)	[-339;-71]	2.6 (±1.27)	[-338.65;-71.25]	0.34	7.9
d_{prec}	$T_{2m\ prec}$	Weighted annual, all data	22 (±8)	[11;35]	0.36 (±0.16)	[10.62;34.88]	0.39	0.9

Table S5. Local meteoric water lines (LMWLs) computed over different time periods using ECHAM6-wiso outputs.

Regression variables		Data used	Intercept		Slope		r^2	CV RMSE
Dependent	Indipendent		β_0 (±std. error)	BS 95th CI	β_1 (±std. error)	BS 95th CI		‰
δ^2H	$\delta^{18}O$	Daily, all data	-12 (±1)	[-15;-8]	7.66 (±0.02)	[7.6;7.73]	0.99	9
δ^2H	$\delta^{18}O$	Daily, winter (JJA)	-24 (±2)	[-30;-16]	7.49 (±0.04)	[7.39;7.64]	0.98	9.5
δ^2H	$\delta^{18}O$	Daily, spring (SON)	-16 (±2)	[-19;-12]	7.63 (±0.03)	[7.56;7.7]	0.99	7.5
δ^2H	$\delta^{18}O$	Daily, summer (DJF)	-12 (±2)	[-16;-9]	7.54 (±0.04)	[7.46;7.63]	0.99	5.9
δ^2H	$\delta^{18}O$	Daily, autumn (MAM)	-20 (±2)	[-28;-2]	7.48 (±0.03)	[7.34;7.81]	0.98	9.4
δ^2H	$\delta^{18}O$	Monthly, all data	3 (±2)	[-1;7]	7.94 (±0.04)	[7.86;8.02]	1.00	3.5
δ^2H	$\delta^{18}O$	Monthly, winter (JJA)	-17 (±8)	[-36;-2]	7.62 (±0.14)	[7.3;7.87]	0.99	2.8
δ^2H	$\delta^{18}O$	Monthly, spring (SON)	-2 (±4)	[-12;6]	7.9 (±0.07)	[7.7;8.04]	1.00	2.7
δ^2H	$\delta^{18}O$	Monthly, summer (DJF)	-6 (±6)	[-17;5]	7.68 (±0.14)	[7.43;7.95]	0.99	3
δ^2H	$\delta^{18}O$	Monthly, autumn (MAM)	3 (±10)	[-23;22]	7.89 (±0.18)	[7.42;8.22]	0.99	2.8
δ^2H_{prec}	$\delta^{18}O_{prec}$	Weighted monthly, all data	10 (±3)	[4;15]	8.1 (±0.06)	[7.99;8.21]	0.99	3.8
δ^2H_{prec}	$\delta^{18}O_{prec}$	Weighted monthly, winter (JJA)	-10 (±9)	[-24;-1]	7.74 (±0.17)	[7.5;7.93]	0.99	4
δ^2H_{prec}	$\delta^{18}O_{prec}$	Weighted monthly, spring (SON)	5 (±5)	[-3;17]	8.06 (±0.1)	[7.88;8.32]	1.00	2.9
δ^2H_{prec}	$\delta^{18}O_{prec}$	Weighted monthly, summer (DJF)	5 (±7)	[-16;17]	7.95 (±0.18)	[7.45;8.24]	0.99	4
δ^2H_{prec}	$\delta^{18}O_{prec}$	Weighted monthly, autumn (MAM)	1 (±6)	[-10;14]	7.89 (±0.11)	[7.65;8.14]	0.99	2.4
δ^2H	$\delta^{18}O$	Annual	19 (±14)	[-3;41]	8.23 (±0.26)	[7.82;8.63]	0.99	0.9
δ^2H_{prec}	$\delta^{18}O_{prec}$	Weighted annual	27 (±16)	[5;73]	8.48 (±0.35)	[8;9.45]	0.99	1

References

Gerrish, L., Fretwell, P., and Cooper, P.: Medium resolution vector polygons of the Antarctic coastline (Version 7.4) [Data set], https://doi.org/10.5285/ed0a7b70-5adc-4c1e-8d8a-0bb5ee659d18, 2021.

Matsuoka, K., Skoglund, A., Roth, G., de Pomereu, J., Griffiths, H., Headland, R., Herried, B., Katsumata, K., Le Brocq, A., Licht, K., Morgan, F., Neff, P. D., Ritz, C., Scheinert, M., Tamura, T., Van de Putte, A., van den Broeke, M., von Deschwanden, A., Deschamps-Berger, C., Van Liefferinge, B., Tronstad, S., and Melvær, Y.: Quantarctica, an integrated mapping environment for Antarctica, the Southern Ocean, and sub-Antarctic islands, Environ. Model. Softw., 140, https://doi.org/10.1016/j.envsoft.2021.105015, 2021.